Western blot analysis

Protein samples were extracted from tail, liver, brain, and spinal cord and homogenized in buffer containing 0.1% sodium dodecyl sulfate (SDS), 1% Triton X-100, 1% deoxycholate, and 1 m*M* phenylmethylsulfonyl fluoride. Equal amounts of extracted protein were then mixed with Laemmli sample buffer, denatured, and separated on 15% SDS-polyacrylamide gel electrophoresis. After transfer to a polyvinylidine difluoride membrane (Bio-Rad, Hercules, CA), blots were probed with anti-SOD1 polyclonal antibody S-100 (Assay Designs, Ann Arbor, MI) or anti-β-actin monoclonal antibody (Sigma, St. Louis, MO) and then visualized using enhanced chemiluminescence. Densitometric analysis was performed using Image J application software with the amounts of SOD1 being normalized for β-actin.

Quantitative reverse transcription-PCR

Total RNA was extracted from liver samples using Isogen (Nippon Gene, Tokyo, Japan), and 1 μg of total RNA from each sample was reverse-transcribed to cDNA using the High Capacity RNA-to-cDNA kit (Applied Biosystems, Carlsbad, CA). cDNA was used for quantitative reverse transcription-PCR (qRT-PCR) using the TaqMan system and the ABI Prism 7700 Sequence Detection system (Applied Biosystems) according to the manufacturers' instructions. The following primers and probe were used to quantify mouse and human SOD1: 5′-GGTGCAGGGAACCATCCA-3′ and 5′-CCCATGC TGGCCTTCAGT-3′ for the mouse primer set, with 5′-AGGC AAGCGGTGAACCAGTTGTGTTG-3′ for the mouse probe; and 5′-CCACACCTTCACTGGTCCATTA-3′ and 5′-CGACG GCCCAGTGCA-3′ for the human primer set, with 5′-TTC CTTCTGCTCGAAATTGATGATGCCC-3′ for the human probe.

Measurement of SOD1 activity

Each liver sample was homogenized in 5 volumes (wt/vol) of homogenization buffer containing 0.25 *M* sucrose, 20 m*M* Tris-HCl, and 1 m*M* EDTA and centrifuged at 78,000 *g* for 60 min. The supernatant was carefully removed and analyzed. To inactivate Mn-SOD, the sample was treated with 2% SDS at 37°C for 30 min. After cooling to 4°C, 0.1 volume of 3 *M* KCl was added, and the mixture was centrifuged at 20,000 *g* for 10 min to remove excess SDS. The supernatant was then assayed for SOD activity using the SOD Assay Kit-WST (Dojindo, Kumamoto, Japan) according to the manufacturer's instructions.

Histological study

For histological observation, formalin-fixed, paraffin-embedded liver sections (4 μm thick) were stained with hematoxylin and eosin, and frozen liver sections (8 μm thick) were stained with Sudan III using standard protocols. To quantify hepatic lipid accumulation, the density of lipid droplets (minimal diameter, >2 μm) was measured on the visual fields of a light microscope.

Serum alanine aminotransferase

Blood was collected from the animals via a retro-orbital plexus bleed, and the alanine aminotransferase (ALT) levels in the serum were measured using the ultraviiolet method.

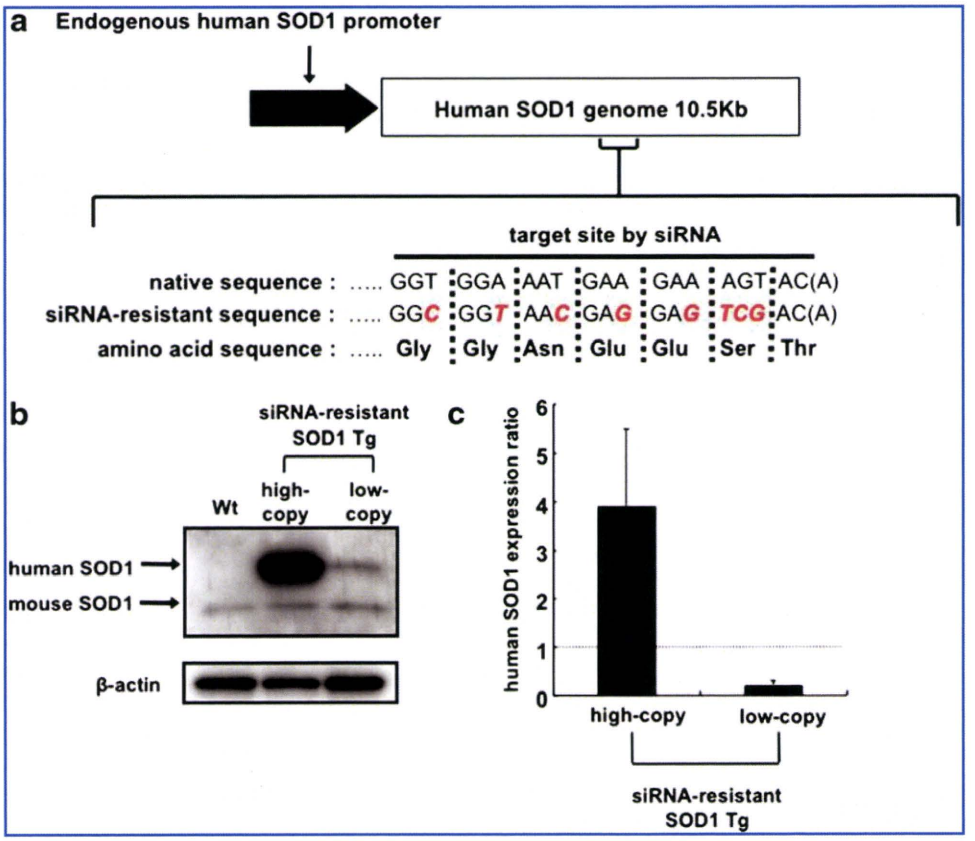

FIG. 1. Generation of siRNA-resistant SOD1 Tg mice. (**a**) Construction of the siRNA-resistant human SOD1 expression vector. The target sequence of anti-SOD1 shRNA is shown below the schematic. The red, italicized letters indicate mutated nucleotides. The amino acid sequence expressed by the siRNA-resistant human SOD1 expression vector is the same as that of the wild-type human SOD1. (**b**) Western blot analysis of SOD1 protein isolated from high-copy and low-copy Tg tails. (**c**) qRT-PCR of human mRNA in the liver. Values are presented as the ratio to endogenous mouse SOD1 mRNA. Data are mean values with SD ($n=3$). Wt, wild-type littermates; high-copy Tg, high-copy siRNA-resistant SOD1 Tg mice; low-copy Tg, low-copy siRNA-resistant SOD1 Tg mice.

Measurements were conducted at Nagahama Life Science Laboratory (Shiga, Japan).

Statistical analysis

Statistical significance was assessed between groups using Student's t test or one-way analysis of variance. Significance was defined as $p < 0.05$.

Results

Generation of siRNA-resistant SOD1 Tg mice

We applied a selective suppression RNAi strategy to rescue the side effects resulting from downregulation of endogenous SOD1 in anti-SOD1 shRNA Tg mice. First, we attempted to generate Tg mice that express wild-type human SOD1 modified to be resistant to the siRNA. The nucleotide sequence

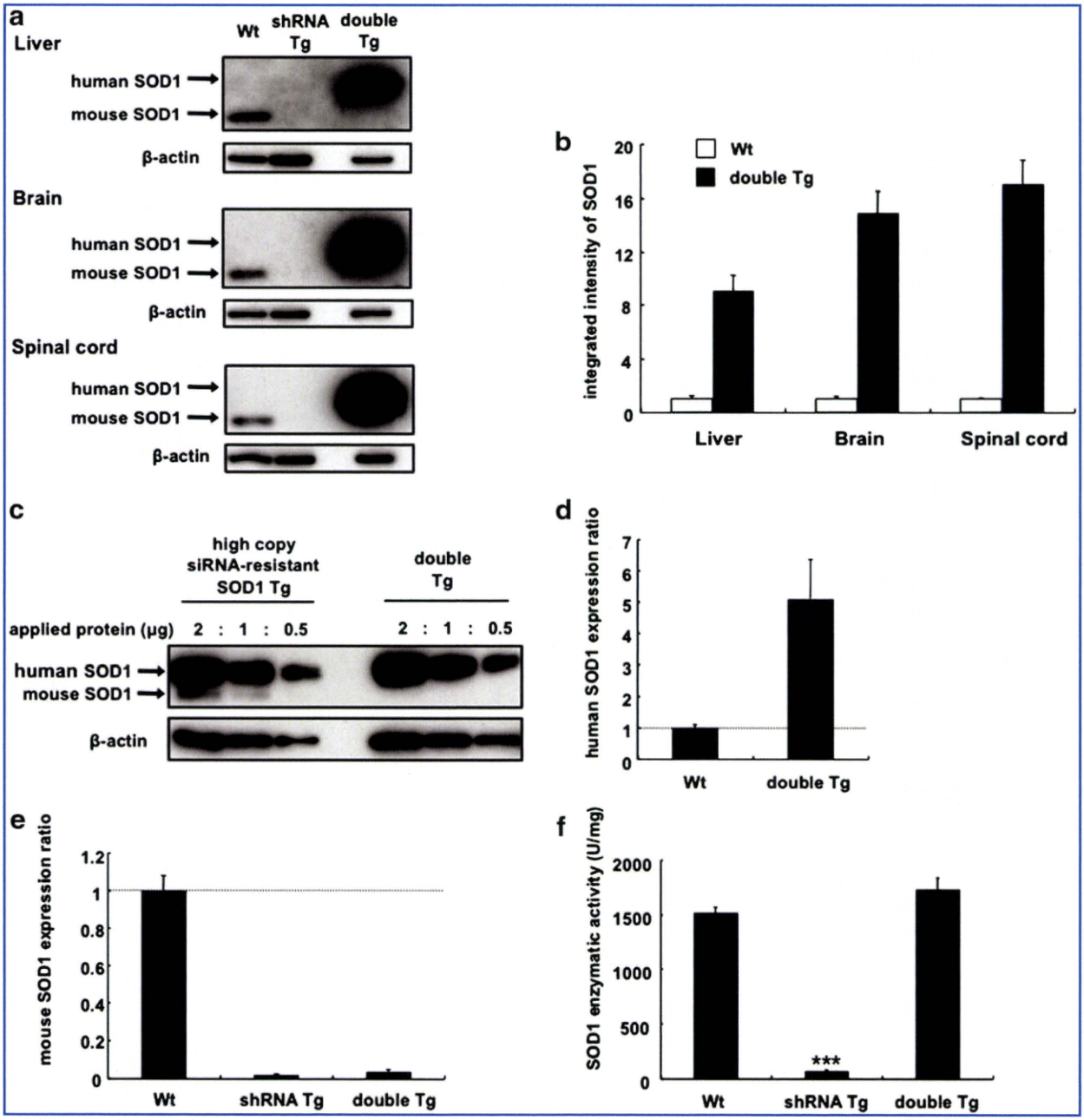

FIG. 2. Restoration of wild-type SOD1 expression in double Tg mice. (**a**) Human SOD1 protein was restored in the liver, brain, and spinal cord of double Tg mice as assessed by western blot analysis. Mouse SOD1 proteins in double Tg mice were reduced as in the anti-SOD1 shRNA Tg mice. (**b**) Corrected densitometry determinations of western blot staining for restored SOD1 protein. Values are presented as the ratio to band intensity of SOD1 protein in wild-type (Wt) littermates. Data are presented as mean values with SD ($n = 3$). (**c**) Human SOD1 protein levels in the liver of high-copy Tg and double Tg mice were similar. (**d**) qRT-PCR of human SOD1 mRNA in the liver. Data are presented as mean values with SD ($n = 3$). (**e**) qRT-PCR of endogenous mouse SOD1 mRNA in double Tg mice. Values are presented as the ratio to endogenous mouse SOD1 mRNA. Data are presented as mean values with SD ($n = 3$). (**f**) SOD1 enzyme activity in the liver. Data are presented as means with SD ($n = 3$ for each group) ***$p < 0.001$. shRNA Tg, anti-SOD1 shRNA Tg mice; double Tg, double Tg mice.

encoded by siRNA-resistant SOD1 was altered to encode the same amino acid sequence as that of native SOD1 (Fig. 1a). Two strains of high- and low-copy siRNA-resistant SOD1 Tg mice were obtained in which the expressed human SOD1 protein levels differed on western blot analysis (Fig. 1b). We also quantified the expression of human and mouse SOD1 mRNA by qRT-PCR using TaqMan probes specific for their respective SOD1 mRNA. The expression level of human SOD1 mRNA in low-copy siRNA-resistant SOD1 Tg mice was approximately one-fifth that of endogenous mouse SOD1 mRNA, whereas that in the high-copy siRNA-resistant SOD1 Tg mice was four times higher than that of mouse SOD1 mRNA (Fig. 1c).

Generation of double Tg mice that express both anti-SOD1 shRNA and siRNA-resistant SOD1

We next attempted to generate double Tg mice by crossing high-copy siRNA-resistant SOD1 Tg mice with anti-SOD1 shRNA Tg mice. In the liver, brain, and spinal cord of double Tg mice, human SOD1 protein was robustly expressed, whereas the endogenous mouse SOD1 protein remained suppressed (Fig. 2a). The corrected band density of SOD1 in wild-type littermates and double Tg mice is shown in Fig. 2b. In double Tg mice, the expression level of human SOD1 protein was almost equal to that of siRNA-resistant high-copy SOD1 Tg mice, indicating that human SOD1 was not inhibited by siRNA (Fig. 2c). The expression level of human SOD1 mRNA in double Tg mice was five times higher than that of endogenous mouse SOD1 mRNA observed in wild-type littermates (Fig. 2d), whereas that of mouse SOD1 mRNA was markedly decreased in anti-SOD1 shRNA Tg mice and double Tg mice by 98.0% and 96.1%, respectively (Fig. 2e). In contrast, the enzymatic activity of SOD1 in the liver of double Tg mice was almost equal to that of the wild-type littermates (Fig. 2f).

Rescue of liver dysfunction in double Tg mice

SOD1 is a major antioxidant, and SOD1 knockout mice exhibit abnormalities such as reduced fertility and enhanced susceptibility to axonal injury and cerebral ischemia (Reaume *et al.*, 1996; Matzuk *et al.*, 1998; Kawase *et al.*, 1999). Furthermore, hepatic lipid accumulation has also been found in SOD1 knockout mice (Uchiyama *et al.*, 2006). Thus, it was considered that oxidative stress enhanced hepatic lipid accumulation by impairing lipoprotein secretion due to the degradation of apolipoprotein B in hepatocytes. Similarly, we observed a significant increase in ALT (Fig. 3a) and the presence of numerous small lipid droplets in the liver of anti-SOD1 shRNA Tg mice (Fig. 3b and c).

In double Tg mice, serum ALT levels were recovered to within the normal range (Fig. 3a). Moreover, the number of lipid droplets in the liver of double Tg mice was decreased to levels similar to that of the wild-type mice as observed on Sudan III staining (Fig. 3b and c). The liver abnormalities identified in anti-SOD1 shRNA Tg mice disappeared in double Tg mice, indicating that loss of wild-type SOD1 function was recovered by the expression of siRNA-resistant SOD1.

Vector-mediated delivery of both anti-SOD1 shRNA and siRNA-resistant SOD1

To achieve conditional *in vivo* knockdown of the target gene with this strategy, we used vector-mediated delivery

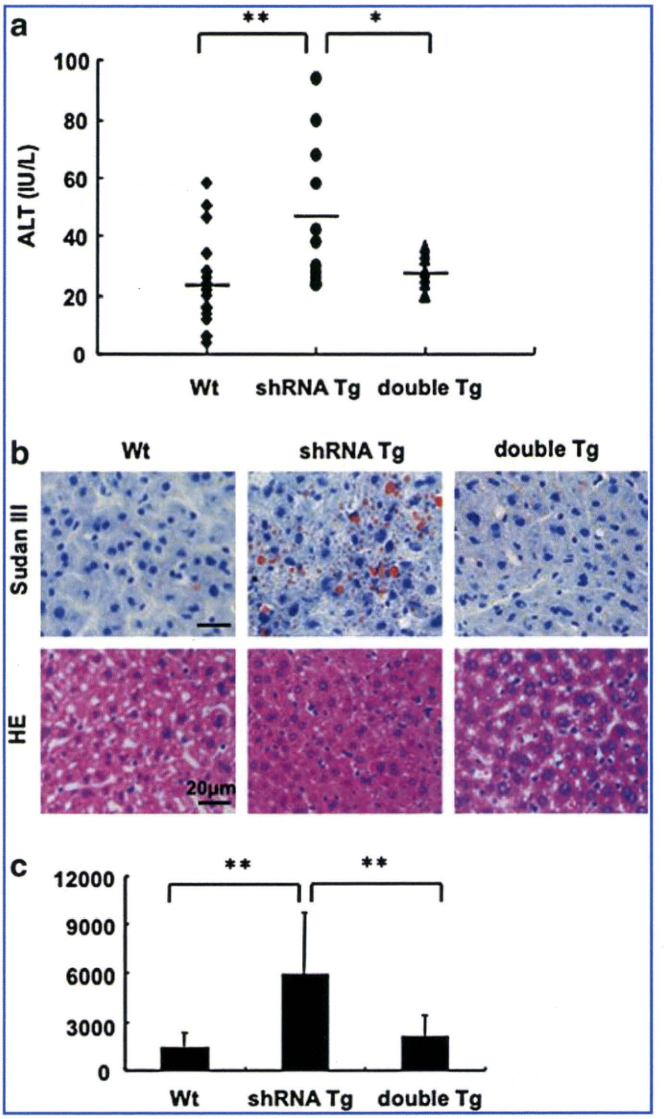

FIG. 3. Disappearance of liver dysfunction in double Tg mice. (**a**) ALT levels in the serum ($n = 20$ for wild-type [Wt] littermates, $n = 11$ for anti-SOD1 shRNA Tg mice, $n = 8$ for double Tg mice). Horizontal bars indicate the mean values. $^{*}p < 0.05$, $^{**}p < 0.01$. (**b**) Histological analysis of the liver. Sections were stained with Sudan III (**upper panel**) and hematoxylin and eosin (HE) (**lower panel**). Scale bar = 20 μm. (**c**) Average number of lipid droplets (>2 μm). Data are presented as mean values with SD. $^{**}p < 0.01$.

with rAAV. In order to introduce both shRNA and siRNA-resistant mRNA to each cell *in vivo*, we generated a construct that dually expressed anti-SOD1 shRNA and siRNA-resistant SOD1 cDNA (pAAV-shRNA/resistant SOD1), as well as shRNA against SOD1 alone (pAAV-shRNA) (Fig. 4a).

$SOD1^{G93A}$ Tg mice were intravenously injected with 1×10^{12} vector genomes per mouse of rAAV-2/8-shRNA or -shRNA/resistant SOD1. Three weeks later, we found that the $SOD1^{G93A}$ Tg mice injected with rAAV-2/8-shRNA demonstrated significant inhibition of both mutant G93A SOD1 and endogenous mouse SOD1 proteins in the liver as assessed by western blot analysis. On the other hand, in $SOD1^{G93A}$ Tg mice injected with rAAV-2/8-shRNA/resistant SOD1, levels

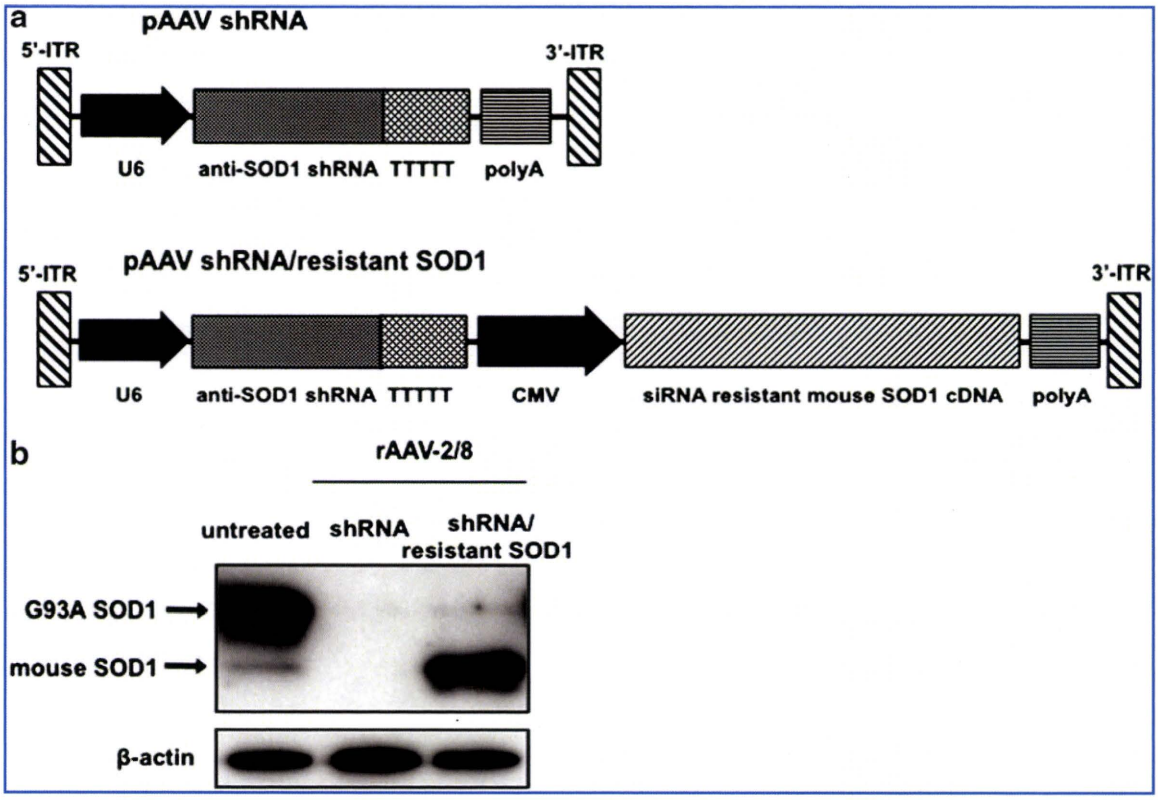

FIG. 4. Vector-mediated delivery of anti-SOD1 shRNA and siRNA-resistant SOD1 cDNA. (**a**) Schematic of constructs packaged in rAAV-2/8 expressing anti-SOD1 shRNA (pAAV shRNA) or co-expressing anti-SOD1 shRNA and siRNA-resistant mouse SOD1 cDNA (pAAV shRNA/resistant SOD1). ITR, inverted terminal repeats. (**b**) Effects of rAAV-2/8 in the liver of SOD1G93A Tg mice assessed by western blot analysis. rAAV-2/8-shRNA or -shRNA/resistant SOD1 was injected into SOD1G93A Tg mice via the tail vein. The mutant G93A SOD1 protein level was reduced, but the wild-type mouse SOD1 protein level was restored in mice treated with the rAAV-2/8-shRNA/resistant SOD1.

of wild-type mouse SOD1 protein were much increased under inhibition of mutant G93A SOD1 protein (Fig. 4b).

Discussion

Our initial reports on our RNAi strategy raised several problems, including (1) the requirement of both siRNA and restored wild-type protein to be delivered to every cell, (2) differences in function that may exist between the endogenous and exogenously expressed proteins, and (3) the control of expression levels of the restored wild-type protein (Kubodera *et al.*, 2005).

In order to express both siRNA and restored wild-type protein in each cell, we constructed a cassette that dually expressed anti-SOD1 shRNA containing U6 promoter and siRNA-resistant wild-type SOD1 cDNA containing CMV promoter in rAAV vectors. Following systemic intravenous injection of this rAAV vector into $SOD1^{G93A}$ Tg mice, mutant G93A SOD1 protein in the liver almost disappeared as seen in mice injected with rAAV vectors expressing anti-SOD1 shRNA alone. In addition, the wild-type mouse SOD1 protein was also restored. As both promoters work ubiquitously, two transcripts should be expressed in each cell. Recently, another vector construct that simultaneously expressed transgene and shRNA was reported (Samakoglu *et al.*, 2006). In this construct, a promoter-less lariat-embedded shRNA sequence was inserted within the intron of the *Pol*II-driven protein-coding transgene, generating efficient shRNA from the processed primary transcript.

In the double transgenic mice, the enzymatic activity of restored siRNA-resistant SOD1 was similar to its endogenous levels, and the side effects observed in the anti-SOD1 shRNA Tg mice disappeared without any other additional side effects. Therefore, the expression level of restored siRNA-resistant SOD1 appeared appropriate for our purpose. However, the level of the restored SOD1 enzymatic activity was much less than expected compared with the overexpressed siRNA-resistant SOD1 mRNA in the double Tg mice. As SOD1 functions in its dimeric form, chimeric dimerization of human and mouse SOD1 may not function as a mouse homodimer. Alternatively, there may be differences in post-translational modifications between recombinant human and endogenous mouse SOD1 in the mouse liver that affects enzymatic activity.

Using rAAV-mediated gene delivery, the protein level of overexpressed wild-type mouse SOD1 in the liver was much greater than the endogenous level. It has been reported that human wild-type SOD1 transgenic mice, unlike mutant SOD1 transgenic mice, do not develop motor abnormalities and paralysis (Gurney *et al.*, 1994; Ripps *et al.*, 1995), while aged mice overexpressing wild-type SOD1 show minor motor abnormalities (Jaarsma *et al.*, 2000). In addition, increased wild-type SOD1 accelerates the phenotype of an ALS mouse model with mutant SOD1 (Deng *et al.*, 2006; Wang *et al.*, 2009).

α-Synuclein, amyloid precursor protein, and peripheral myelin protein-22 are known to cause autosomal dominant disease in the presence of duplication or triplication of a gene locus (Harding, 1995; Singleton *et al.*, 2003; Rovelet-Lecrux *et al.*, 2006), indicating that wild-type protein expression levels should be strictly controlled. The inducible expression system represents one of the possible techniques that can be used to regulate gene expression. A few gene expression systems that can be regulated with a steroid hormone-dependent and tetracycline-dependent transcriptional switch have been reported (Goverdhana *et al.*, 2005; Manfredsson *et al.*, 2009). However, a precise method for tuning the levels of proteins expressed from transgene has not been established.

The major targets of our RNAi strategy are dominantly inherited diseases in which the causative gene normally plays an important role. Recent studies have indicated that mutations in several dominantly inherited diseases, including polyglutamine diseases, prion disease, and Alzheimer's disease, contributed to pathology through both a loss- and gain-of-function (Van Raamsdonk *et al.*, 2005; Harris and True, 2006; Thomas *et al.*, 2006; Shen and Kelleher, 2007; Lim *et al.*, 2008). For example, in the case of spinocerebellar ataxia type 1, which is one of the polyglutamine diseases and caused by the expansion of a glutamine-encoding CAG repeat in the *ataxin-1* gene, ataxin-1 protein forms at least two distinct native complexes. Polyglutamine expansion alters the proportion of the mutant protein participating in the formation of these complexes. One complex then causes disease via a gain-of-function mechanism, whereas the other complex concomitantly causes a loss-of-function (Lim *et al.*, 2008). Our RNAi strategy for allele-specific suppression is suitable for these cases, as concomitant loss of wild-type protein function can be restored in addition to inhibiting the toxicity of the mutant protein. The optimal restored level of the wild-type protein, however, may differ depending on the mechanism of concomitant loss-of-function in each disease.

In conclusion, we present an efficiency of our RNAi strategy for allele-specific suppression *in vivo*, by preventing the side effects due to downregulation of endogenous wild-type protein using Tg mice and furthermore by the mutant allele-specific gene suppression using intravenously administered viral vectors. Although the restored protein level should be specifically determined for each disease, our *in vivo* results indicate that our RNAi strategy is promising for gene therapy of dominantly inherited diseases, especially those exhibiting concomitant loss of wild-type protein function.

Acknowledgments

We thank Dr. Masashi Aoki for providing human SOD1 promoter and cDNA and Dr. James M. Wilson for providing the AAV packaging plasmid. This work was supported in part by grants from the Ministry of Education, Science, Culture, Sports, and Technology, Japan (18659256 and 20790610), the Ministry of Health Labor and Welfare, Japan (2212065), and the 21st Century COE Program on Brain Integration and its Disorders from Tokyo Medical and Dental University.

Author Disclosure Statement

No competing financial interests exist.

References

Bumcrot, D., Manoharan, M., Koteliansky, V., and Sah, D.W. (2006). RNAi therapeutics: A potential new class of pharmaceutical drugs. Nat. Chem. Biol. 2, 711–719.

Deng, H.X., Shi, Y., Furukawa, Y., Zhai, H., Fu, R., Liu, E., Gorrie, G.H., Khan, M.S., Hung, W.Y., Bigio, E.H., Lukas, T., Dal Canto, M.C., O'Halloran, T.V., and Siddique, T. (2006). Conversion to the amyotrophic lateral sclerosis phenotype is associated with intermolecular linked insoluble aggregates of SOD1 in mitochondria. Proc. Natl. Acad. Sci. U.S.A. 103, 7142–7147.

Dykxhoorn, D.M., Palliser, D., and Lieberman, J. (2006a). The silent treatment: siRNAs as small molecule drugs. Gene Ther. 13, 541–552.

Dykxhoorn, D.M., Schlehuber, L.D., London, I.M., and Lieberman, J. (2006b). Determinants of specific RNA interference-mediated silencing of human beta-globin alleles differing by a single nucleotide polymorphism. Proc. Natl. Acad. Sci. U.S.A. 103, 5953–5958.

Elbashir, S.M., Harborth, J., Lendeckel, W., Yalcin, A., Weber, K., and Tuschl, T. (2001). Duplexes of 21-nucleotide RNAs mediate RNA interference in cultured mammalian cells. Nature 411, 494–498.

Gonzalez-Alegre, P., Miller, V.M., Davidson, B.L., and Paulson, H.L. (2003). Toward therapy for DYT1 dystonia: Allele-specific silencing of mutant TorsinA. Ann. Neurol. 53, 781–787.

Goverdhana, S., Puntel, M., Xiong, W., Zirger, J.M., Barcia, C., Curtin, J.F., Soffer, E.B., Mondkar, S., King, G.D., Hu, J., Sciascia, S.A., Candolfi, M., Greengold, D.S., Lowenstein, P.R., and Castro, M.G. (2005). Regulatable gene expression systems for gene therapy applications: Progress and future challenges. Mol. Ther. 12, 189–211.

Gurney, M.E., Pu, H., Chiu, A.Y., Dal Canto, M.C., Polchow, C.Y., Alexander, D.D., Caliendo, J., Hemtati, A., Kwon, Y.W., Deng, H.X., Chen, W., Zhai, P., Sufit, R.L., and Siddique, T. (1994). Motor neuron degeneration in mice that express a human Cu,Zn superoxide dismutase mutation. Science 264, 1772–1775.

Harding, A.E. (1995). From the syndrome of Charcot, Marie and Tooth to disorders of peripheral myelin proteins. Brain 118, 809–818.

Harris, D.A., and True, H.L. (2006). New insights into prion structure and toxicity. Neuron 50, 353–357.

Jaarsma, D., Haasdijk, E.D., Grashorn, J.A., Hawkins, R., Van Duijn, W., Verspaget, H.W., London, J., and Holstege, J.C. (2000). Human Cu/Zn superoxide dismutase (SOD1) overexpression in mice causes mitochondrial vacuolization, axonal degeneration, and premature motoneuron death and accelerates motoneuron disease in mice expressing a familial amyotrophic lateral sclerosis mutant SOD1. Neurobiol. Dis. 7, 623–643.

Kawase, M., Murakami, K., Fujimura, M., Morita-Fujimura, Y., Gasche, Y., Kondo, T., Scott, R.W., and Chan, P.H. (1999). Exacerbation of delayed cell injury after transient global ischemia in mutant mice with CuZn superoxide dismutase deficiency. Stroke 30, 1962–1968.

Kim, D.H., and Rossi, J.J. (2007). Strategies for silencing human disease using RNA interference. Nat. Rev. Genet. 8, 173–184.

Kubodera, T., Yokota, T., Ishikawa, K., and Mizusawa, H. (2005). New RNAi strategy for selective suppression of a mutant allele in polyglutamine disease. Oligonucleotides 15, 298–302.

Li, Y., Yokota, T., Matsumura, R., Taira, K., and Mizusawa, H. (2004). Sequence-dependent and independent inhibition specific for mutant ataxin-3 by small interfering RNA. Ann. Neurol. 56, 124–129.

Lim, J., Crespo-Barreto, J., Jafar-Nejad, P., Bowman, A.B., Richman, R., Hill, D.E., Orr, H.T., and Zoghbi, H.Y. (2008).

Opposing effects of polyglutamine expansion on native protein complexes contribute to SCA1. Nature 452, 713–718.

Manfredsson, F.P., Burger, C., Rising, A.C., Zuobi-Hasona, K., Sullivan, L.F., Lewin, A.S., Huang, J., Piercefield, E., Muzyczka, N., and Mandel, R.J. (2009). Tight long-term dynamic doxycycline responsive nigrostriatal GDNF using a single rAAV vector. Mol. Ther. 17, 1857–1867.

Matzuk, M.M., Dionne, L., Guo, Q., Kumar, T.R., and Lebovitz, R.M. (1998). Ovarian function in superoxide dismutase 1 and 2 knockout mice. Endocrinology 139, 4008–4011.

Miller, V.M., Xia, H., Marrs, G.L., Gouvion, C.M., Lee, G., Davidson, B.L., and Paulson, H.L. (2003). Allele-specific silencing of dominant disease genes. Proc. Natl. Acad. Sci. U.S.A. 100, 7195–7200.

Miller, V.M., Gouvion, C.M., Davidson, B.L., and Paulson, H.L. (2004). Targeting Alzheimer's disease genes with RNA interference: An efficient strategy for silencing mutant alleles. Nucleic Acids Res. 32, 661–668.

Ohnishi, Y., Tamura, Y., Yoshida, M., Tokunaga, K., and Hohjoh, H. (2008). Enhancement of allele discrimination by introduction of nucleotide mismatches into siRNA in allele-specific gene silencing by RNAi. PLoS ONE 3, e2248.

Pasinelli, P., and Brown, R.H. (2006). Molecular biology of amyotrophic lateral sclerosis: Insights from genetics. Nat. Rev. Neurosci. 7, 710–723.

Reaume, A.G., Elliott, J.L., Hoffman, E.K., Kowall, N.W., Ferrante, R.J., Siwek, D.F., Wilcox, H.M., Flood, D.G., Beal, M.F., Brown, R.H., Jr., Scott, R.W., and Snider, W.D. (1996). Motor neurons in Cu/Zn superoxide dismutase-deficient mice develop normally but exhibit enhanced cell death after axonal injury. Nat. Genet. 13, 43–47.

Ripps, M.E., Huntley, G.W., Hof, P.R., Morrison, J.H., and Gordon, J.W. (1995). Transgenic mice expressing an altered murine superoxide dismutase gene provide an animal model of amyotrophic lateral sclerosis. Proc. Natl. Acad. Sci. U.S.A. 92, 689–693.

Rovelet-Lecrux, A., Hannequin, D., Raux, G., Le Meur, N., Laquerriere, A., Vital, A., Dumanchin, C., Feuillette, S., Brice, A., Vercelletto, M., Dubas, F., Frebourg, T., and Campion, D. (2006). APP locus duplication causes autosomal dominant early-onset Alzheimer disease with cerebral amyloid angiopathy. Nat. Genet. 38, 24–26.

Saito, Y., Yokota, T., Mitani, T., Ito, K., Anzai, M., Miyagishi, M., Taira, K., and Mizusawa, H. (2005). Transgenic small interfering RNA halts amyotrophic lateral sclerosis in a mouse model. J. Biol. Chem. 280, 42826–42830.

Samakoglu, S., Lisowski, L., Budak-Alpdogan, T., Usachenko, Y., Acuto, S., Di Marzo, R., Maggio, A., Zhu, P., Tisdale, J.F., Riviere, I., and Sadelain, M. (2006). A genetic strategy to treat sickle cell anemia by coregulating globin transgene expression and RNA interference. Nat. Biotechnol. 24, 89–94.

Sasaguri, H., Mitani, T., Anzai, M., Kubodera, T., Saito, Y., Yamada, H., Mizusawa, H., and Yokota, T. (2009). Silencing efficiency differs among tissues and endogenous microRNA pathway is preserved in short hairpin RNA transgenic mice. FEBS Lett. 583, 213–218.

Schwarz, D.S., Ding, H., Kennington, L., Moore, J.T., Schelter, J., Burchard, J., Linsley, P.S., Aronin, N., Xu, Z., and Zamore, P.D. (2006). Designing siRNA that distinguish between genes that differ by a single nucleotide. PLoS Genet. 2, e140.

Shen, J., and Kelleher, R.J., 3rd (2007). The presenilin hypothesis of Alzheimer's disease: Evidence for a loss-of-function pathogenic mechanism. Proc. Natl. Acad. Sci. U.S.A. 104, 403–409.

Singleton, A.B., Farrer, M., Johnson, J., Singleton, A., Hague, S., Kachergus, J., Hulihan, M., Peuralinna, T., Dutra, A., Nussbaum, R., Lincoln, S., Crawley, A., Hanson, M., Maraganore, D., Adler, C., Cookson, M.R., Muenter, M., Baptista, M., Miller, D., Blancato, J., Hardy, J., and Gwinn-Hardy, K. (2003). alpha-Synuclein locus triplication causes Parkinson's disease. Science 302, 841.

Taymans, J.M., Vandenberghe, L.H., Haute, C.V., Thiry, I., Deroose, C.M., Moretelmans, L., Wilson, J.M., Debyser, Z., and Baekelandt, V. (2007). Comparative analysis of adeno-associated viral vector serotypes 1, 2, 5, 7, and 8 in mouse brain. Hum. Gene Ther. 18, 195–206.

Thomas, P.S., Jr., Fraley, G.S., Damian, V., Woodke, L.B., Zapata, F., Sophier, B.L., Plymate, S.R., and La Spada, A.R. (2006). Loss of endogenous androgen receptor protein accelerates motor neuron degeneration and accentuates androgen insensitivity in a mouse model of X-linked spinal and bulbar muscular atrophy. Hum. Mol. Genet. 15, 2225–2238.

Uchiyama, S., Shimizu, T., and Shirasawa, T. (2006). CuZn-SOD deficiency causes ApoB degradation and induces hepatic lipid accumulation by impaired lipoprotein secretion in mice. J. Biol. Chem. 281, 31713–31719.

van Bilsen, P.H., Jaspers, L., Lombardi, M.S., Odekerken, J.C., Burright, E.N., and Kaemmerer, W.F. (2008). Identification and allele-specific silencing of the mutant huntingtin allele in Huntington's disease patient-derived fibroblasts. Hum. Gene Ther. 19, 710–719.

Van Raamsdonk, J.M., Pearson, J., Rogers, D.A., Bissada, N., Vogl, A.W., Hayden, M.R., and Leavitt, B.R. (2005). Loss of wild-type huntingtin influences motor dysfunction and survival in the YAC128 mouse model of Huntington disease. Hum. Mol. Genet. 14, 1379–1392.

Wang, L., Deng, H.X., Grisotti, G., Zhai, H., Siddique, T., and Roos, R.P. (2009). Wild-type SOD1 overexpression accelerates disease onset of a G85R SOD1 mouse. Hum. Mol. Genet. 18, 1642–1651.

Xia, X.G., Zhou, H., Zhou, S., Yu, Y., Wu, R., and Xu, Z. (2005). An RNAi strategy for treatment of amyotrophic lateral sclerosis caused by mutant Cu,Zn superoxide dismutase. J. Neurochem. 92, 362–367.

Yokota, T., Miyagishi, M., Hino, T., Matsumura, R., Tasinato, A., Urushitani, M., Rao, R.V., Takahashi, R., Bredesen, D.E., Taira, K., and Mizusawa, H. (2004). siRNA-based inhibition specific for mutant SOD1 with single nucleotide alternation in familial ALS, compared with ribozyme and DNA enzyme. Biochem. Biophys. Res. Commun. 314, 283–291.

Yokota, T., Sasaguri, H., Saito, Y., Yamada, H., Unno, T., Yamamoto, Y., Kubodera, T., Anzai, M., Mitani, T., and Mizusawa, H. (2007). Increase of disease duration of amyotrophic lateral sclerosis in a mouse model by transgenic small interfering RNA. Arch. Neurol. 64, 145–146.

Address correspondence to:
Dr. Takanori Yokota
Department of Neurology and Neurological Science
Tokyo Medical and Dental University
1-5-45 Yushima, Bunkyo-ku, Tokyo 113-8519, Japan

E-mail: tak-yokota.nuro@tmd.ac.jp

Received for publication March 14, 2010;
accepted after revision July 19, 2010.

Published online: July 20, 2010.

LGI3 interacts with flotillin-1 to mediate APP trafficking and exosome formation

Sachi Okabayashi[a,b] and Nobuyuki Kimura[a]

We recently showed that leucine-rich glioma inactivated 3 (LGI3) mediates the internalization of β-amyloid protein and transferrin, a well-known marker for clathrin-dependent endocytosis, in neural cells. These findings strongly suggest that LGI3 is involved in the endocytosis system in the brain; however, the precise function of LGI3 remains unclear. Here, we show that LGI3 interacts with flotillin-1 (Flo1), and RNA interference analysis shows that LGI3 stabilized Flo1, and Flo1 also stabilized LGI3 *vice versa*. Moreover, the downregulation of the LGI3/Flo1 complex altered β-amyloid precursor protein trafficking directly to late endosomes and disrupted exosome formation, suggesting that LGI3 is involved not only in endocytosis but also in another intracellular transport system through binding with its co-factor such as Flo1. *NeuroReport* 21:606–610 © 2010 Wolters Kluwer Health | Lippincott Williams & Wilkins.

NeuroReport 2010, 21:606–610

Keywords: β-amyloid precursor protein, clathrin, endocytosis, flotillin-1, leucine-rich glioma inactivated 3

[a]Laboratory of Disease Control, Tsukuba Primate Research Center, National Institute of Biomedical Innovation and [b]The Corporation for Production and Research of Laboratory Primates, Hachimandai, Tsukuba-shi, Ibaraki, Japan

Correspondence to Dr Nobuyuki Kimura, PhD, DVM, Laboratory of Disease Control, Tsukuba Primate Research Center, National Institute of Biomedical Innovation, 1-1 Hachimandai, Tsukuba-shi, Ibaraki 305-0843, Japan
Tel: +81 29 837 2121; fax: +81 29 837 0218; e-mail: kimura@nibio.go.jp

Received 20 January 2010 **accepted** 31 January 2010

Introduction

We have shown earlier that β-amyloid protein (Aβ) upregulates leucine-rich glioma inactivated 3 (LGI3) in cultured rat astrocytes [1]. Aβ is the major component of senile plaques, which are a characteristic feature of Alzheimer's disease [2]. Recently, we showed that LGI3 mediates the internalization of Aβ and transferrin, a well-known marker for clathrin (CLA)-dependent endocytosis in neural cells [3].

These findings strongly suggest that LGI3 is involved in the endocytosis system in the brain.

How glial cells take up Aβ remains controversial, and a recent study showed that Aβ internalization does not depend on CLA or caveolae [4]. Flotillin-1 (Flo1) is associated with noncaveolar membrane microdomains and has been recently shown to be a defining component of a CLA-independent and caveolin-independent endocytic pathway in mammalian cells [5]. Thus, in this study, we investigated the relationship between LGI3 and Flo1 or CLA. Here, we show that LGI3 interacts with Flo1 in the brain, and RNA interference studies showed that the LGI3/Flo1 complex mediates β-amyloid precursor protein (APP) trafficking and exosome formation.

Methods

Co-immunoprecipitation

C57BL/6 mice were purchased from SLC Japan (Shizuoka, Japan), and cortices from 10-week-old mice were used for co-immunoprecipitation in this study.

All steps were performed at 4°C unless otherwise noted. For immunoprecipitation, we used Dynabeads Protein G (Invitrogen, Carlsbad, California, USA). Mouse brains were homogenized in lysis buffer consisting 25 mM Tris–HCl (pH 8.0), 0.5% Triton X-100, 0.5% Nonidet P-40, and a Complete Mini proteinase inhibitor cocktail, and then centrifuged at 100 000*g* for 15 min. The precleaned supernatant containing 500 μg of proteins was incubated with goat polyclonal anti-Flo1 (Flo1g; Santa Cruz Biotechnology, Santa Cruz, California, USA) or goat IgG (Southern Biotechnology, Birmingham, Alabama, USA) for 2 h. After immunoreaction, the antibody-linked supernatant was incubated with precleaned beads for 1 h. The protein was eluted from the beads with an electrophoresis sample buffer, and then subjected to western blot analyses as described earlier [1]. We used the following primary antibodies: rabbit polyclonal anti-LGI3 [1] and rabbit polyclonal anti-Flo1 (Flo1r; Santa Cruz Biotechnology). We performed three independent experiments by using different mouse brains (see Supplementary Figure, Supplemental digital content 1, *http://links.lww.com/WNR/A52*).

All animal experiments were carried out according to the National Institute of Biomedical Innovation rules and guidelines for experimental animal welfare.

RNA interference

Mouse neuroblastoma Neuro2a cells were cultured in a culture medium (Dulbecco's Modified Eagle's Medium with 10% fetal calf serum). The cells were plated at 1.5×10^4 cells/cm^2 onto 12-well plates (Wako, Osaka, Japan) for

Supplemental digital content is available for this article. Direct URL citations appear in the printed text and are provided in the HTML and PDF versions of this article on the journal's Website (*www.neuroreport.com*).

DOI: 10.1097/WNR.0b013e3283383467

western blot analyses, or plated at 1.0×10^4 cells/cm^2 onto 2-well LAB-TEK chamber slides (Nalge Nunc, Rochester, New York, USA) for immunocytochemistry.

For double-stranded RNA-mediated interference (RNAi) studies, we used the following short double-stranded RNAs (siRNAs) against LGI3 (siLGI3), Flo1 (siFlo1), and clathrin heavy chain (siCLA): siLGI3, 5′-CCGUUGC UAGCGUGUCUGAGU-3′ (sense) and 5′-UCAGACACG CUAGCAACGGAG-3′ (antisense); siFlo1, 5′-CUAGUGG AAGCGGAACCAUGG-3′ (sense) and 5′-AUGGUUCCG CUUCCACUAGAC-3′ (antisense); siCLA, 5′-GCUACU UAGUCCGUCGAAAGG-3′ (sense) and 5′-UUUCGACG GACUAAGUAGCGA-3′ (antisense). To avoid off-target effects, all siRNAs were carefully designed by Enhanced siDirect. The control siRNA had a random sequence. RNAi experiments were performed by using siLentFect lipid reagent (BioRad, Hercules, California, USA), according to the manufacturer's protocol.

Seventy-two hours after siRNA transfection, cells (12-well plates) were lysed in a sample buffer solution containing 62.5 mM Tris–HCl (pH 6.8), 2 mM EDTA, 0.5% Triton X-100, 2% SDS, and proteinase inhibitor cocktail to extract total cellular proteins. Total proteins were adjusted to 10 μg, and then subjected to western blot analyses. We used the following primary antibodies: anti-LGI3 [1]; mouse monoclonal anti-β-actin (Sigma, St Louis, Missouri, USA); anti-Flo1r; anti-CLAm; rabbit polyclonal anti-APP (Zymed, Carlsbad, California, USA); mouse monoclonal antisecreted fragment of APP by α-secretase (sAPPα; IBL, Gunma, Japan); and rabbit polyclonal antisecreted fragment of APP by β-secretase (sAPPβ; IBL). The anti-APP antibody used in this study recognizes both full-length APP and C-terminal fragment of APP by α-secretase (αCTF) or β-secretase (βCTF). Immunoreactive bands were quantified with commercially available software (Quantity One, PDI, Inc., Upper Saddle River, New Jersey, USA), and one-way analyses of variance were performed followed by the Bonferroni/Dunn post-hoc test. We performed three independent experiments ($N = 6$ for each experimental group), duplicating each experiment.

Cells plated on chamber slides were fixed with 4% paraformaldehyde and then permeabilized with 0.5% Tween 20. After blocking with 3% bovine serum albumin, the cells were incubated overnight at 4°C with the following primary antibodies: anti-LGI3; anti-Flo1g; anti-CLAm; anti-APP; rabbit polyclonal anti-sortilin (Applied Biological Materials, Richmond, Canada); rabbit polyclonal anti-TrkB (Santa Cruz Biotechnology); mouse monoclonal anti-Rab7 (Abcam, Cambridge, Massachusetts, USA); and mouse monoclonal anti-Golgi (Abcam). The cells were then incubated with AlexaFluor-conjugated secondary antibodies (Invitrogen), followed by a DAPI nuclear stain (Santa Cruz Biotechnology) for 1 h at room temperature. All cells were examined with a Digital Eclipse C1 confocal microscope (Nikon, Kanagawa, Japan).

Preparation of extracellular membrane fractions and immunoblotting for medium-derived sAPPα

Seventy-two hours after siRNA treatment, extracellular membrane fractions were prepared from the culture medium (12-well plates) as described elsewhere [6]. The resulting pellets were resuspended in the sample buffer, and then subjected to western blot analyses. We used the following primary antibodies: mouse monoclonal anti-Alix (Santa Cruz Biotechnology), anti-Flo1r, and mouse monoclonal anti-transferrin receptor (TfR; Zymed). In addition, to assess the levels of sAPPα secreted from the cells, culture media were subjected to ultracentrifugation at 100 000*g* for 1 h. The resulting pellets were resuspended in the sample buffer, and then subjected to immunoblotting with anti-sAPPα1. We examined 12 independent samples for each group.

Results

LGI3 interacts with Flo1 in the brain

In mouse neuroblastoma Neuro2a cells, Flo1 almost completely colocalized with LGI3; however, CLA partly colocalized with LGI3 near the plasma membrane (Fig. 1a). To assess whether LGI3 interacts with Flo1 *in vivo*, we performed co-immunoprecipitation using mouse brain homogenates. In the mouse brain, several anti-LGI3-specific immunoreactive bands were detected as reported earlier [7], and an approximately 70 kDa form of LGI3 was immunoprecipitated with an anti-Flo1 antibody (Fig. 1b).

Next, we performed RNAi studies to assess whether LGI3 is required for the stability of the complex. Western blot analyses confirmed that our siRNAs successfully downregulated each target in the Neuro2a cells (Fig. 1c). The depletion of LGI3 induced significant downregulation of Flo1, and the depletion of Flo1 also induced downregulation of LGI3 and *vice versa* (Fig. 1c). By contrast, we did not observe such a relationship between LGI3 and CLA (Fig. 1c). Immunocytochemistry confirmed that the Flo1 immunoreactivity diminished in LGI3-depleted cells, whereas CLA immunoreactivity persisted (data not shown).

LGI3/Flo1 complex mediates APP trafficking

Flo1 is associated with a lipid raft, and growing evidence suggests that lipid raft-associated proteins mediate APP endocytosis and cleavage [8–10]. These findings prompted us to investigate whether the LGI3/Flo1 complex mediates APP endocytosis and/or cleavage. As APP cleavage by β-secretase mainly occurs through an endocytic pathway [7], we first investigated the sAPPβ and βCTF levels. The depletion of Flo1 or LGI3 clearly decreased the amount of both sAPPβ and βCTF (Fig. 2a and b).

Fig. 1

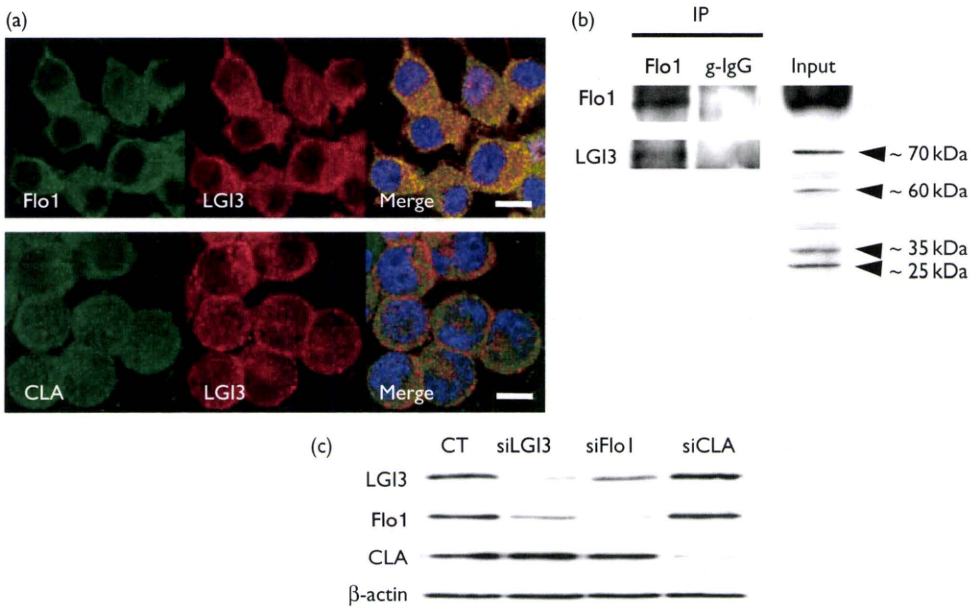

(a) Photomicrographs of Neuro2a cells immunostained for LGI3, Flo1, and CLA. Flo1 almost completely colocalized with LGI3, however, CLA partly colocalized with LGI3 near plasma membrane. Scale bars, 10 μm. (b) In mouse brain, several anti-LGI3-specific immunoreactive bands were detected, and co-immunoprecipitation analysis showed that a 70 kDa (approx.) form of LGI3 interacts with Flo1; g-IgG, control goat IgG. (c) Western blots showing the amount of LGI3, Flo1, CLA, and β-actin in extracts from Neuro2a cells 72 h after siRNA treatment. The amount of LGI3, Flo1, and CLA clearly dropped 72 h after transfection with each specific siRNA, respectively. The depletion of LGI3 resulted in the concurrent downregulation of Flo1, and the depletion of Flo1 also induced downregulation of LGI3 vice versa. CT, cells transfected with control siRNA; siLGI3, cells transfected with siLGI3; siFlo1, cells transfected with siFlo1; siCLA, cells transfected with siCLA.

APP can be alternately cleaved by α-secretase at plasma membranes [11]. Unexpectedly, the depletion of Flo1 or LGI3 also decreased the amount of both sAPPα and αCTF (Fig. 2a and b). We also confirmed the decrease of sAPPα released into the culture medium (Fig. 2c).

Immunocytochemistry showed that the depletion of LGI3 altered the intracellular localization of APP, and APP clearly accumulated near the nucleus in LGI3-depleted cells (Fig. 2d). Double immunocytochemistry showed that the accumulated APP is localized to Rab7-positive endosomes (Fig. 2d) but not to Golgi (data not shown). The depletion of LGI3 did not alter the localization of sortilin (Fig. 2d) or TrkB (data not shown).

LGI3/Flo1 complex mediates exosome formation in neuronal cells

Flo1 is also associated with exosome membranes [6]. To test whether exosome formation is affected by the depletion of LGI3/Flo1 complex, we prepared extracellular membrane fractions from siRNA-transfected cells. In contrast to control siRNA-transfected cells, the amount of Alix, another marker for exosome membranes, was significantly decreased in both cell lysates and extracellular membrane fractions from LGI3-depleted cells (Fig. 3). However, the depletion of LGI3 did not affect the amount of TfR (Fig. 3).

Discussion

In this study, we showed that LGI3 interacts with Flo1 in the brain and that the LGI3/Flo1 complex mediates APP trafficking and exosome formation. Co-immunoprecipitation analyses revealed that an approximately 70 kDa form of LGI3 interacts with Flo1 (Fig. 1b). A full-length LGI3 is considered to be an approximately 60 kDa protein [1,3], and an approximately 35 kDa truncated form of LGI3 is predominant in the Neuro2a cells (data not shown). Although additional investigations are needed, the truncated LGI3 might dimerize and then interact with Flo1 in the mouse brain. This idea would be supported by the recent finding that syntaxin-1 associates with an approximately 35 kDa truncated form of LGI3, not full-length LGI3, in the mouse brain [7].

Most notably, our RNA interference studies showed that the LGI3/Flo1 complex mediates APP trafficking in the neuronal cells (Fig. 2). As we showed earlier that LGI3 mediates Aβ and transferrin internalization [3], we first assumed that LGI3 is also involved in APP endocytosis. The depletion of LGI3 or Flo1 clearly decreased β-site cleavage products, indicating that APP endocytosis is disturbed (Fig. 2a and b). However, surprisingly, the depletion of LGI3 or Flo1 also decreased α-site cleavage products (Fig. 2b and c). α-site cleavage is considered to occur at plasma membranes before the endocytosis

Fig. 2

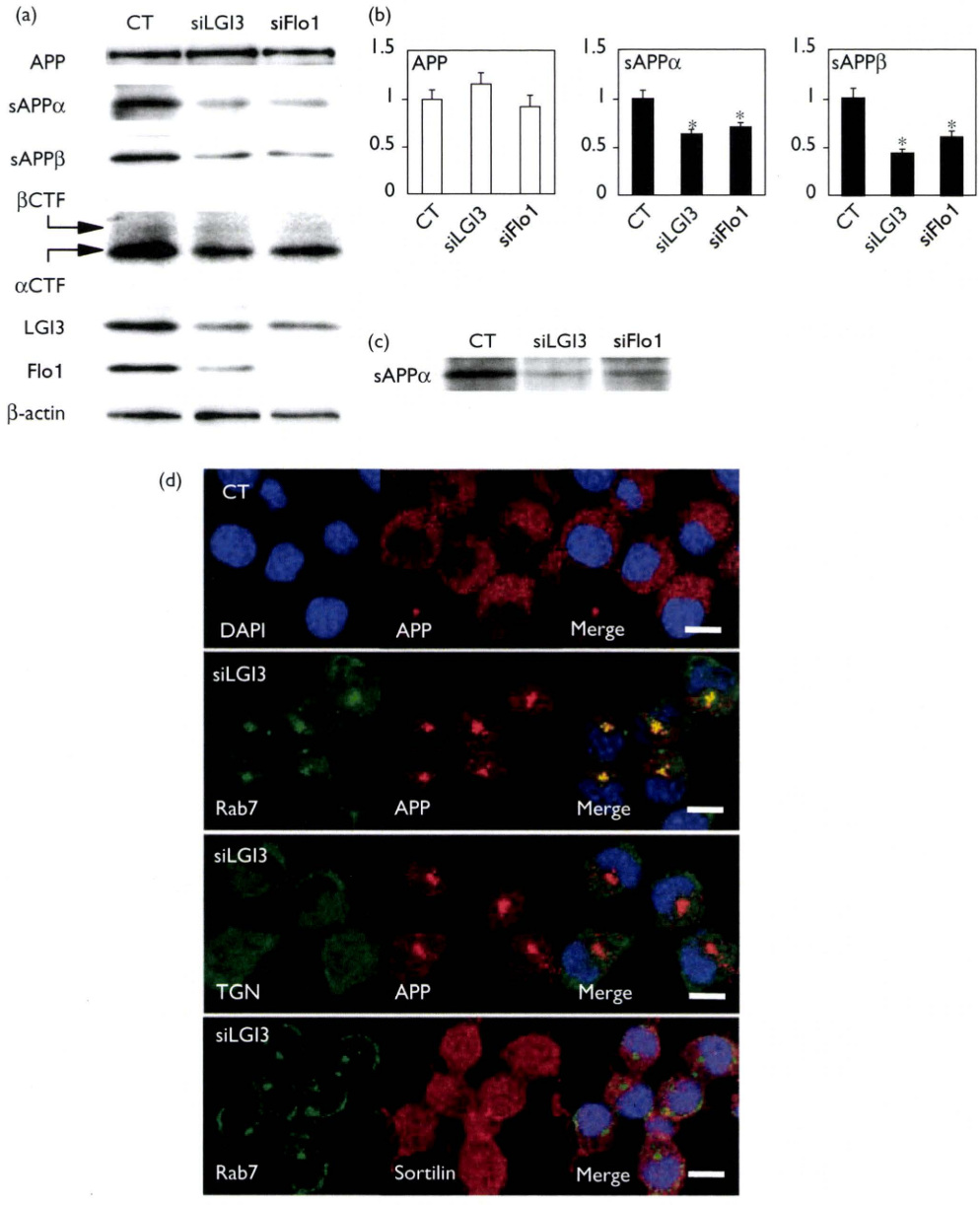

(a) Western blots showing the amount of APP, sAPPα, sAPPβ, αCTF, βCTF, LGI3, Flo1, and β-actin in Neuro2a cells 72 h after siRNA transfection. In LGI3- and Flo1-depleted cells, the amount of sAPPα, sAPPβ, αCTF, and βCTF was appreciably decreased. (b) Histograms showing the effect of LGI3 and Flo1 depletion on the amounts of full-length APP, sAPPα, and sAPPβ in Neuro2a cells. All data were normalized according to β-actin levels. Values are means ± SD. $*P<0.001$. Y-axes show the mean values of the quantified data. (c) Western blots showing the amount of sAPPα released into culture media 72 h after siRNA transfection. (d) Photomicrographs of Neuro2a cells 72 h after siRNA transfection. In siLGI3-transfected cells, APP clearly accumulated near the nucleus, localizing to Rab7-positive endosomes, however, sortilin remained unchanged. Scale bars, 10 μm.

of APP [11], suggesting that APP may not be trafficked to the plasma membrane as a result of the depletion of LGI3/Flo1 complex.

Immunocytochemistry showed that APP accumulated near the nuclei in LGI3-depleted cells, localizing to Rab7-positive endosomes, i.e., late endosomes (Fig. 2d). Cation-dependent mannose 6-phosphate receptor, a major late endosomal protein, is transported from the trans-Golgi network to late endosomes [12], suggesting that proteins can be transported directly to late endosomes from the secretory pathway. Western blot analyses confirmed that the molecular weight of full-length APP was approximately 110 kDa, even in LGI3-depleted or Flo1-depleted cells, suggesting that APP maturation through the secretory pathway is not disturbed. Thus,

Fig. 3

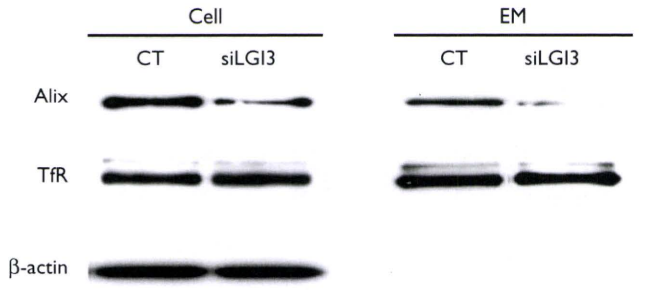

Western blots showing the amount of Alix, transferrin receptor (TfR), and β-actin in whole-cell extracts (Cell) and extracellular membrane (EM) fractions from Neuro2a cells 72 h after siRNA transfection. LGI3 depletion significantly decreased the levels of Alix in both Cell and EM. By contrast, LGI3 depletion did not affect the amount of TfR.

the depletion of the LGI3/Flo1 complex may alter APP trafficking from trans-Golgi network directly to late endosomes but not to the plasma membrane. Moreover, as the depletion of the LGI3/Flo1 complex did not alter the localization of another transmembrane protein, such as sortilin (Fig. 2d), the LGI3/Flo1 complex may mediate APP trafficking specifically.

As Flo1 is associated with exosome membranes [6], it is reasonable that LGI3 is also associated with exosome membranes. This would explain why LGI3 is detected as a secreted protein in the culture medium [13]. Moreover, the depletion of the LGI3/Flo1 complex significantly decreased the amount of Alix, another exosome membrane marker, in both cell lysates and extracellular membrane fractions (Fig. 3a). This finding suggests that the LGI3/Flo1 complex is required for exosome formation itself. As the depletion of LGI3 failed to affect the amount of TfR in the extracellular membrane fractions (Fig. 3), LGI3/Flo1 may not mediate the recycling endocytic pathway.

It is unclear how LGI3 is involved in CLA-dependent endocytosis. An earlier study showed that the depletion of Flo1 did not affect transferrin uptake in HeLa cells [5]. In this study, immunocytochemistry revealed that LGI3 partly colocalizes with CLA near the plasma membranes (Fig. 1a). Although additional investigations are needed, a population of LGI3 molecules may associate with CLA independently of Flo1, and these LGI3/CLA complexes might work only when endocytosis occurs. Overall, the results of this study suggest that LGI3 is involved not only in endocytosis but also in other intracellular transport systems through binding with co-factors such as Flo1.

Conclusion

LGI3 interacts with Flo1 in the brain, and LGI3/Flo1 mediates APP trafficking and exosome formation in neuronal cells. This line of research would provide a great contribution to reveal the details of the intracellular transport system and even the secretion pathway in the brain.

Acknowledgements

This study was supported by a grant-in-aid from the Ministry of Health, Labor, and Welfare, and the Ministry of Education, Culture, Sports, Science, and Technology, Japan.

References

1 Kimura N, Ishii Y, Suzaki S, Negishi T, Kyuwa S, Yoshikawa Y. Aβ upregulates and colocalizes with LGI3 in rat cultured astrocytes. *Cell Mol Neurobiol* 2007; **27**:335–350.
2 Glenner GG. Alzheimer's disease: its proteins and genes. *Cell* 1988; **2**:307–308.
3 Okabayashi S, Kimura N. LGI3 is involved in Aβ uptake by astrocytes and endocytosis itself. *Neuroreport* 2008; **19**:1175–1179.
4 Saavedra L, Mohamed A, Ma V, Kar S, De Chaves EP. Internalization of beta-amyloid peptide by primary neurons in the absence of apolipoprotein E. *J Biol Chem* 2007; **282**:35722–35732.
5 Glebov OO, Bright NA, Nichols BJ. Flotillin-1 defines a clathrin-independent endocytic pathway in mammalian cells. *Nat Cell Biol* 2006; **8**:46–54.
6 Rajendran L, Honsho M, Zahn TR, Keller P, Geiger KD, Verkade P, Simons K. Alzheimer's disease beta-amyloid peptides are released in association with exosomes. *Proc Natl Acad Sci U S A* 2006; **103**:11172–11177.
7 Park WJ, Lee SE, Kwon NS, Baek KJ, Kim DS, Yun HY. Leucine-rich glioma inactivated 3 associates with syntaxin 1. *Neurosci Lett* 2008; **444**:240–244.
8 Schneider A, Rajendran L, Honsho M, Gralle M, Donnert G, Wouters F, *et al.* Flotillin-dependent clustering of the amyloid precursor protein regulates its endocytosis and amyloidogenic processing in neurons. *J Neurosci* 2008; **28**:2874–2882.
9 Ehehalt R, Keller P, Haass C, Thiele C, Simons K. Amyloidogenic processing of the Alzheimer beta-amyloid precursor protein depends on lipid rafts. *J Cell Biol* 2003; **160**:113–123.
10 Fuentealba RA, Barría MI, Lee J, Cam J, Araya C, Escudero CA, *et al.* ApoER2 expression increases Abeta production while decreasing Amyloid Precursor Protein (APP) endocytosis: possible role in the partitioning of APP into lipid rafts and in the regulation of gamma-secretase activity. *Mol Neurodegener* 2007; **2**:14.
11 Sisodia SS. Beta-amyloid precursor protein cleavage by a membrane-bound protease. *Proc Natl Acad Sci U S A* 1992; **89**:6075–6079.
12 Rohrer J, Schweizer A, Johnson KF, Kornfeld S. A determinant in the cytoplasmic tail of the cation-dependent mannose 6-phosphate receptor prevents trafficking to lysosomes. *J Cell Biol* 1995; **130**:1297–1306.
13 Senechal KR, Thaller C, Noebels JL. ADPEAF mutations reduce levels of secreted LGI1, a putative tumor suppressor protein linked to epilepsy. *Hum Mol Genet* 2005; **14**:1613–1620.

BRAIN RESEARCH 1315 (2010) 137–149

available at www.sciencedirect.com

ScienceDirect

www.elsevier.com/locate/brainres

BRAIN RESEARCH

Research Report

Alzheimer-type tau pathology in advanced aged nonhuman primate brains harboring substantial amyloid deposition

Naoto Oikawa[a], *Nobuyuki Kimura*[b], *Katsuhiko Yanagisawa*[a,*]

[a]*Department of Alzheimer's Disease Research, National Institute for Longevity Sciences, National Center for Geriatrics and Gerontology, 36-3, Gengo, Morioka, Obu, Aichi 474-8522, Japan*

[b]*Laboratory of Disease Control, Tsukuba Primate Research Center, National Institute of Biomedical Innovation, 1-1, Hachimandai, Tsukuba-shi, Ibaraki 305-0843, Japan*

ARTICLE INFO

Article history:
Accepted 1 December 2009
Available online 8 January 2010

Keywords:
Alzheimer disease
Amyloid β-protein
Tau
Tau phosphorylation
Argyrophilic tangle
Dystrophic neurite
Cynomolgus monkey

ABSTRACT

We elucidated how Alzheimer-type pathologies of amyloid β-protein (Aβ) and tau spatiotemporally emerge in brains of nontransgenic nonhuman primate, cynomolgus monkey, in the present study. To examine the accumulation of deposited Aβ, phosphorylated tau accumulation, intracellular tau accumulation, and neurofibrillary tangle formation, the brains, mainly temporal cortex and hippocampus, of 34 cynomolgus monkeys aged 6 to 36 years were studied by biochemical and histochemical analyses. Biochemically, first, the accumulation of insoluble Aβ was detected in the neocortical (temporal and frontal) and hippocampal regions of animals as young as mid-20s and their levels were extremely high in those of advanced age. The accumulation of phosphorylated tau in the same regions occurred before the age of 20 with poor correlation to the levels of insoluble Aβ. Histologically, intraneuronal and intraoligodendroglial tau accumulation was observed in temporal cortex and hippocampus of animals before the age of 20. In an advanced aged 36-year-old individual, argyrophilic tangles and tau-accumulated dystrophic neurites were markedly observed in the medial temporal area contiguous to limbic structures. Notably, these tau pathologies also emerged, to a lesser extent, in the temporal cortices of advanced aged animals harboring significant amounts of insoluble Aβ. These results suggest that the cynomolgus monkey can be used to elucidate the age-dependent sequence of Aβ and tau pathologies.

1. Introduction

The emergence of numerous senile plaques (SPs), neurofibrillary tangles (NFTs), and neuronal loss are hallmarks of Alzheimer disease (AD). The main component of SPs is amyloid β-protein (Aβ), which is a 39- to 43-residue protein with heterogeneity at their carboxy-termini. Among them, Aβ40 and Aβ42 terminating at Val-40 and Ala-42, respectively, are major forms (Mori et al., 1992; Roher et al., 1993). On the other hand, NFTs are mainly composed of a microtubule-associated protein, tau (Grundke-Iqbal et al., 1986, Ihara et al., 1986), with hyperphosphorylation (Flament et al., 1989, Lee et al., 1991).

* *Corresponding author.* Fax: +81 562 44 6594.
E-mail address: katuhiko@ncgg.go.jp (K. Yanagisawa).

Abbreviations: AD, Alzheimer disease; Aβ, amyloid β-protein; SP, senile plaque; NFT, neurofibrillary tangle; APP, amyloid precursor protein; NHP, nonhuman primate

0006-8993/$ – see front matter © 2009 Elsevier B.V. All rights reserved.
doi:10.1016/j.brainres.2009.12.005

Fundamental questions regarding the pathogenesis of AD is how Aβ and tau are integrated into SPs and NFTs, respectively, and how these pathological assemblies are relevant to neuronal death. Moreover, it remains unclear whether the formations of SPs and NFTs are linked or mutually independent. To date, enormous efforts have been made to elucidate these issues using various animal models, particularly transgenic (Tg) mice. In the analysis of processes underlying Aβ pathology in AD, the Tg mice harboring the familial AD-related mutations in *amyloid precursor protein (APP)* gene and *presenilin* genes have been extensively studied (for review, Duyckaerts et al., 2008). In the analysis of processes underlying tau pathology in AD, alternative Tg mice harboring the mutations relating to other tauopathies, including frontotemporal dementia and parkinsonism linked to chromosome 17 (FTDP-17), in *tau* gene have been studied (for review, Frank et al., 2008). Furthermore, triple Tg mice harboring mutations in *APP*, *presenilin*, and *tau* genes are fascinating because these mice show synaptic dysfunction in addition to the formation of both SPs and NFTs (Oddo et al., 2003). These Tg mice are indeed valuable models for studying AD pathogenesis; however, it has been argued that the pathological sequences observed in these mice are different from those in AD brain. The differences may be attributed to alterations in the expression levels of APP and tau, which could occur through genetic manipulations. For example, Aβ is overproduced far beyond the physiological extent in APP-Tg mice owing to the enhanced expression of mutant APP, resulting in high loads of soluble Aβ prior to the development of any Aβ pathology (Kawarabayashi et al., 2001; Kuo et al., 2001).

Nontransgenic animals, such as nonhuman primates (NHPs) and nonprimate mammalian species, are also available for studying the pathogeneses of Aβ and tau. Distinct from Tg mice, both the production of Aβ and expression of tau are likely within physiological ranges in nontransgenic animals; thus, the natural spatiotemporal profiles of Aβ and tau pathologies should be presented in the brains of these animals. To date, it has been reported that a lot of mammalian species exhibit cerebral Aβ-amyloidosis, such as parenchymal Aβ deposition and amyloid angiopathy, and intraneuronal tau accumulation (Bons et al., 2006; Braak et al., 1994; Cummings et al., 1996a,b; Gearing et al., 1994; Geula et al., 2002; Härtig et al., 2000; Lemere et al., 2004, 2008; Podlisny et al., 1991; Roertgen et al., 1996; Schultz et al., 2000a,b; Selkoe et al., 1987; Walker et al., 1987). Among those animals, we paid particular attention to cynomolgus monkey because of the similarity of Aβ pathology as follows. First, cored plaque is the major type in the monkey brain (Nakamura et al., 1998). Second, the number of Aβ42-composed plaques is higher than that of Aβ40-composed ones in the parenchyma, whereas the amyloid angiopathies are equally immunostained with anti-Aβ42 antibody and anti-Aβ40 antibody, respectively (Nakamura et al., 1995). However, it has not been clarified whether Aβ is deposited in the brain in age-dependent and region-specific manners. Tau pathology has also been previously studied in cynomolgus monkey brain (Kiatipattanasakul et al., 2000; Kimura et al., 2003, 2007; Nakamura et al., 1996a,b). Among them, tangle formation in neurons and glial cells was reported in one case although this case may be atypical because the animal showed some neurological deficit and tangles were detected only in subcortical regions (Kiatipattanasakul et al., 2000). Despite these previous studies, it remains to be determined whether Aβ pathology and tau pathology in the brain independently occur or are mutually related in cynomolgus monkey brains.

In this study, we biochemically and histologically characterized the profiles of Aβ and tau pathologies in detail in the brains of cynomolgus monkeys aged 6 to 36 years old. Here, we report that Alzheimer-type tau pathology can occur in advanced aged brains, even in neocortices, harboring substantial amounts of insoluble Aβ.

2. Results

2.1. *Age-dependent and region-specific insoluble Aβ deposition in the brains*

To determine whether Aβ deposition occurs in age-dependent and region-specific manners in the brains of NHP, we biochemically examined 33 temporal cortices and 19 hippocampi obtained from monkeys aged from 6 to 36 years (temporal cortices) and from 17 to 36 years (hippocampi). In a serial Western blotting analysis of those, insoluble Aβ was initially detected in the animals in their mid-20s, whereas insoluble Aβ was not detectable in animals under the age of 22 years in temporal cortices and of 24 years in hippocampi (Fig. 1A. The data for animals aged 6 and 14 years are not shown). In general, accumulation of insoluble Aβ occurred in an age-dependent manner; however, the levels of insoluble Aβ were variable from animal to animal. Some animals even over the mid-20s did not show any Aβ deposition. Notably, the level of insoluble Aβ was extremely high in two animals over the age of 30 (32-c and 36-c). To confirm the result of biochemical examination, we performed immunohistochemistry on the temporal cortices of the animals under the age of 20 (17-a), mid-20s (25-b), and over the age of 30 (32-c and 36-c). In accordance with the results of biochemical analysis, the immunohistochemical study revealed a small and large number of Aβ-immunoreactive plaques in the sections of the animal aged 25 years (25-b) and over the age of 30 (36-c), respectively, whereas no Aβ-immunoreactivity was observed in the animal aged 17 years (17-a) (Fig. 1B). In addition to the samples of the temporal cortex and hippocampus, we also biochemically examined the insoluble Aβ in the frontal and occipital cortices and cerebellum of the animals in their mid-20s. The levels of insoluble Aβ were high in the samples of frontal and temporal cortices, whereas that of the occipital cortices was very low (Fig. 1C). On the other hand, no insoluble Aβ were detected in the cerebella (Fig. 1C).

2.2. *Level of soluble Aβ in the brains*

Soluble fraction of brain homogenates were analyzed to detect soluble Aβ on 16 temporal cortices and 9 hippocampi of the animals aged from 14 to 36 years (temporal cortices) and from 25 to 36 years (hippocampi). Soluble Aβ was not detected in the most analyzed samples; however, the Aβ was detected only in the animals over the age of 30, which showed extremely high levels of insoluble Aβ deposition (Supplemental Fig. 1A). The

data for animals aged from 14 to 24 years are not shown. To explore the source of the soluble Aβ and estimate the contribution of the levels of soluble Aβ to the deposition of insoluble Aβ in the brain, we performed Western blotting analyses of soluble and insoluble fractions obtained from identical samples of brains of monkeys aged over 30 and of APP-Tg mice, Tg2576, aged 13.5 months. In contrast to the sample of APP-Tg mouse brains, in which comparable levels of soluble and insoluble Aβ were detected, soluble Aβ was detected at only negligible levels, despite the extremely high levels of insoluble Aβ, in the samples of monkey brains (Supplemental Fig. 1B).

2.3. *Deposited, insoluble Aβ species in the brains*

To determine which species of Aβ initially and favorably deposited in the monkey brains, we performed Western blotting analysis using the anti-Aβ40 and Aβ42 antibodies in the temporal cortices of five animals aged 24 to 32 years. In accordance with the result of a previous report (Nakamura et al., 1995), the levels of insoluble Aβ42 were apparently higher than those of Aβ40 in almost all samples except one, 25-c, in which the levels of Aβ42 and Aβ40 were comparable (Supplemental Fig. 2A). In the Western blotting using an anti-pyroglutamate Aβ (N3pE-Aβ) antibody (Supplemental Fig. 2B), the immunoreactivity was detected at a significant level only in the sample obtained from the animal aged 32 years, 32-c, which contained an extremely high level of insoluble Aβ42 (Supplemental Fig. 2A).

2.4. *Accumulation of soluble phosphorylated tau in the brains*

We performed Western blotting analysis of the soluble fractions of the temporal cortex and hippocampus using 2B11, and then we assessed the levels of tau phosphorylation by estimating the mobility shift of the immunoreactive bands based on the results of the samples that were treated for enzymatic dephosphorylation prior to Western blotting (Fig. 2A). With this procedure, it was revealed that phosphory-

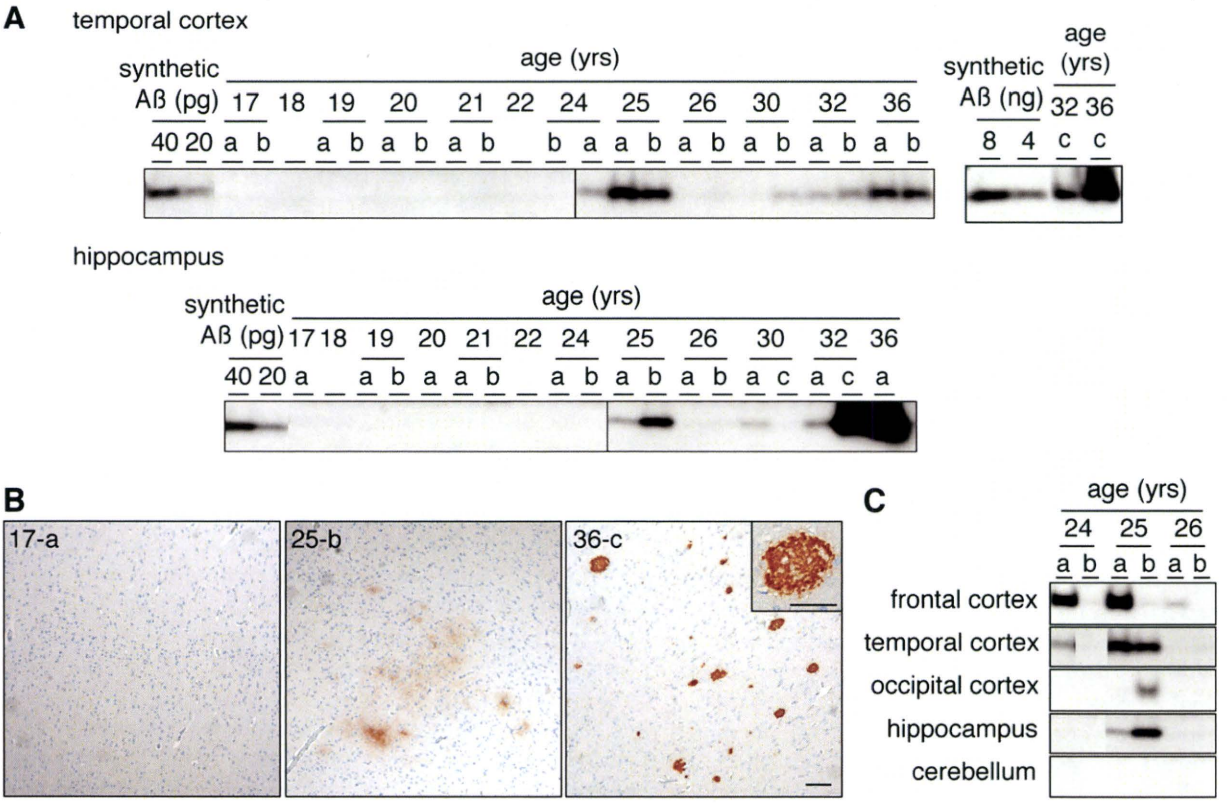

Fig. 1 – Age-dependent and region-dependent insoluble Ab deposition in monkey brains. (A) Western blots of TBS-insoluble Aβ in the samples of temporal cortices (upper panels) and hippocampi (lower panel) of cynomolgus monkey brains. Samples from monkeys aged 17 to 36 years were analyzed. Note that only two samples of temporal cortices, 32-c and 36-c, were examined in a normal manner, not in a highly sensitive manner, so that the order was different from the other blots (upper right panel). The small letters (a, b, and c) written under the ages indicate individual monkeys. (B) Immunohistochemistry using anti-Aβ antibody [anti-human amyloid β (N)] in temporal cortices of 17-a, 25-b, and 36-c. Scale bar, 50 μm (inset of 36-c) and 100 μm. (C) Western blots of TBS-insoluble Aβ in the samples of frontal, temporal, and occipital cortices, hippocampus, and cerebellum. The samples from monkeys aged 24 to 26 years were analyzed. The panels of temporal cortex and hippocampus are the same as those of panel A. In Western blotting, the applied samples were normalized to the tissue wet weight (0.3 mg/sample). Aβ band at 4 kDa was detected using 6E10. Synthetic Aβ1-40 was loaded in each blot.

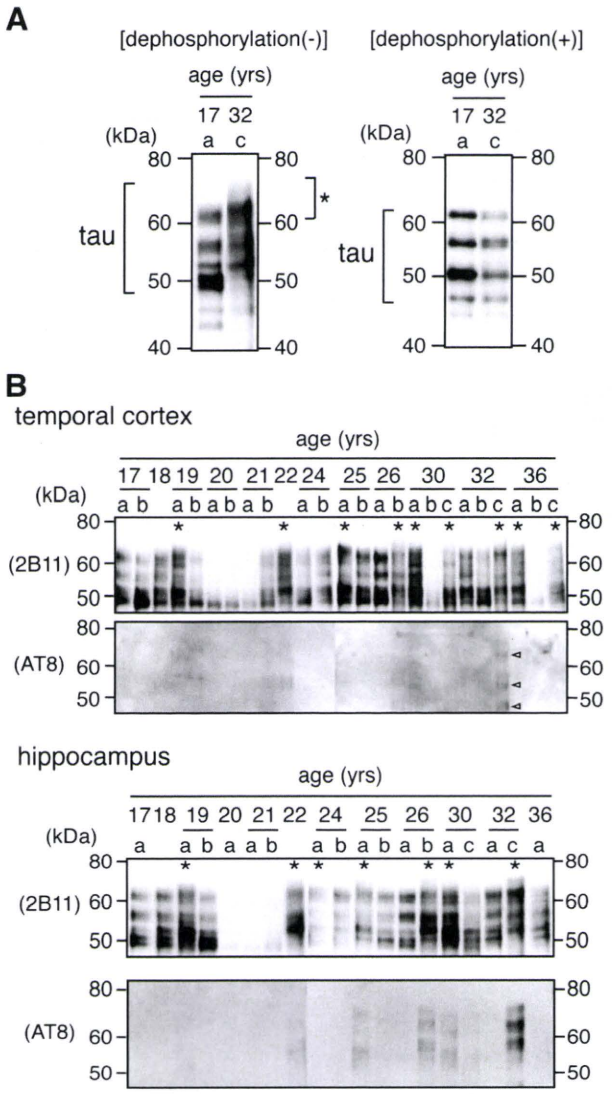

Fig. 2 – Phosphorylation state of TBS-soluble tau in the temporal cortex and hippocampus of monkey brains. (A) Representative pictures of Western blots of hippocampal samples using anti-tau antibody (2B11). Tau bands are indicated by a black square bracket on the left side. The mobility shifts of bands were assessed focusing on the area indicated by an asterisk (left panel). On the same samples, dephosphorylated samples were blotted (right panel). The small letters (a, b, and c) written under the ages indicate individual monkeys. (B) Western blots using 2B11 (upper panel), and anti-phospho-tau antibody, AT8 (lower panel), of the temporal cortical and hippocampal samples without dephosphorylation prior to Western blotting. Asterisks indicate the individuals in whom the mobility shifts of tau bands, mentioned in panel A, were observed. Arrowheads in the blot of the temporal cortical samples indicate AT8-immunoreactive bands.

lated tau accumulated in both the temporal cortex and hippocampus of the brains of animals before the age of 20 (Fig. 2B). We also performed Western blotting using AT8 to search for tau phosphorylation. The AT8-reactive bands were detected in several samples, in which accumulation of phosphorylated tau was also observed using 2B11, and the intensity of AT8-reactive bands increased in an age-dependent manner in the hippocampus (Fig. 2B).

To correlate between the levels of deposited Aβ and accelerated tau phosphorylation (Table 1), the accumulation of phosphorylated tau preceded Aβ deposition as a function of age both in the temporal cortex and hippocampus. Moreover, the accumulation of phosphorylated tau appeared to be independent of the level of Aβ deposition in the monkey brain. However, it was intriguing that abnormally phosphorylated tau, which was detected using AT8, only significantly accumulated in the brains showing extremely high levels of Aβ deposition.

2.5. *Intracellular accumulation of tau in the brains*

To examine the accumulation of tau in the cell with age, we performed immunohistochemical analysis of total tau using 2B11. In the case of 17-a, in which the accumulation of phosphorylated tau, which was determined by the mobility shift of 2B11-reacted tau bands, was negligible in the Western blotting (Fig. 2B), no 2B11 immunoreactivity was observed in the temporal cortex (Fig. 3A) or the hippocampus (data not shown). Whereas in 19-a, in which the accumulation of phosphorylated tau was observed in the Western blotting, the 2B11 immunoreactivity was readily observed in a considerable number of neurons and some glial cells, in the temporal cortex (Fig. 3B) and the hippocampus (data not shown). In animals over the age of 20 (26-a, 26-b, 32-a, 32-c, and 36-c), the number of 2B11-positive glial cells increased with age in good accordance with the result of Western blotting (Figs. 2B and 3C, Table 2). However, 2B11-positive neurons were not detected in the sections of the animals aged over 20 except 36-c, in which strong 2B11 immunoreactivities were occasionally observed in neurons, glial cells, and in clustered dystrophic neurites in the temporal cortex (Figs. 3E–G). The same immunostaining pattern was obtained with HT7, which recognizes residues positioned from 159 to 163 of tau and is expected to detect total tau (data not shown). To characterize 2B11-positive glial cells, we performed double immunostaining of total tau and GFAP (glial fibrillary acidic protein) or Olig2 as markers for astrocytes and oligodendrocytes, respectively. Nearly all 2B11-immunopositive glial cells were Oilg2 immunoreactive (Fig. 3D) and devoid of GFAP immunoreactivity (data not shown).

To investigate whether phosphorylated tau is accumulated in the cell, we also performed immunohistochemical analysis using AT8, which selectively recognizes abnormally phosphorylated tau, in the temporal cortices and hippocampi of the animals, examined in the experiment shown in Fig. 4. In the samples from animals under the age of 30, AT8 immunoreactivity was not detected except in 26-b, in which faint immunoreactivities were detected in a moderate number of glial cells in the temporal cortex, particularly in deeper layers (Fig. 4A). The number of glial cells with the faint immunoreactivities with AT8 in the temporal cortex of 32-c was larger than that of 26-b (26-b, about 34 cells/mm^2; 32-c, about 90 cells/mm^2). Those AT8-positive glial cells were also immunostained with anti-Olig2 antibody but not with anti-GFAP antibody

Table 1 – Biochemical and quantitative profile of Aβ deposition and tau phosphorylation in the brain homogenates.

		19-a	22	24-a	25-a	25-b	26-b	30-a	32-a	32-b	32-c	36-a	36-c
Temporal cortex	Aβ	–	–	+	++	++	–	–	+	+	+++	++	+++
	tau	+	+	–	+	–	+	+	–	–	+*	+	+
Hippocampus	Aβ	–	–	–	+	++	–	+	+	NE	+++	+++	NE
	tau	+	+*	+	+**	–	+**	+**	–	NE	+***	–	NE

The amount of deposited Aβ, that is investigated in Western blotting analysis using 6E10, in the samples is indicated as follows: –, negligible; +, slight; ++, moderate; +++, remarkable. Presence or absence of tau phosphorylation, which was determined with the mobility shift of the 2B11-immunoreactive bands, is indicated as (+) or (–), respectively. Asterisks indicate the levels of AT8 immunoreactivities: *, slight; **, moderate; ***, remarkable; NE, not examined.

(data not shown). In the temporal cortex and hippocampus of 32-a, a neurite-like structure and glial cells were occasionally immunostained with AT8 (Fig. 4B). Notably, the immunostaining of glial cells was strong. In addition, clustered dystrophic neurites were also detected with AT8 in the temporal cortex of 32-c (Fig. 4C). Moreover, some neurons were strongly immunostained with AT8 in the temporal cortex of 36-c (Fig. 4D).

2.6. *Formation of argyrophilic structures in the advanced aged monkey brains*

To explore the formation of argyrophilic tangles in monkey brains, we performed Gallyas silver staining, which is known to be a highly specific silver-staining method for detecting NFTs (for a review, see Uchihara, 2007) of the temporal cortices

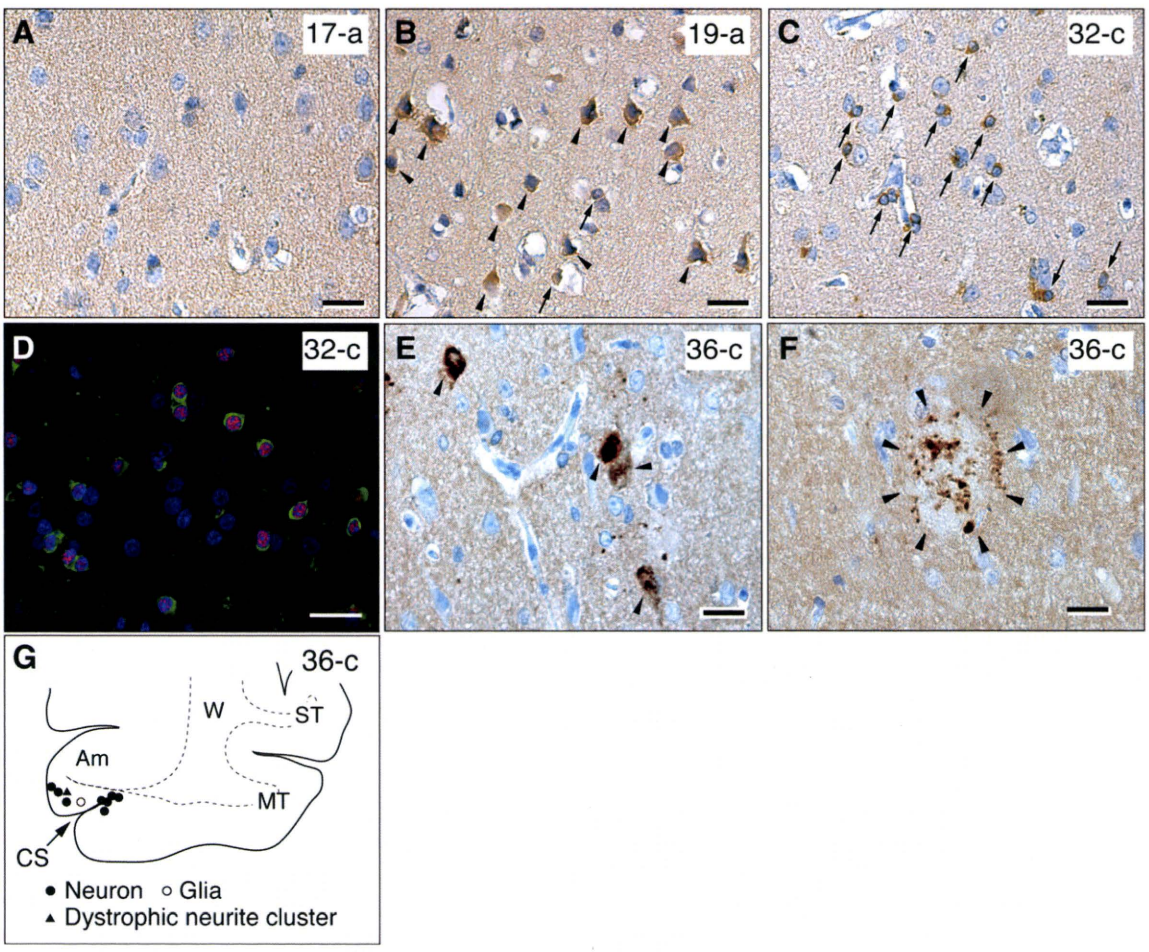

Fig. 3 – Accumulation of tau in neurons and glial cells in the temporal cortices of monkey brains. (A-C, E, and F) Immunoperoxidase staining of temporal cortices using 2B11 with counterstaining using hematoxylin. A, 17-a; B, 19-a; C, 32-c; E and F, 36-c. Arrows and arrowheads indicate 2B11-positive glial cells and neurons, respectively. 2B11-positive dystrophic neurite cluster is indicated by arrowheads. (D) Double immunofluorescence labelling of temporal cortex of 32-c using 2B11 (green) and anti-Olig2 antibody (red), which reacts with nuclear protein, Oilg2, of oligodendrocytes. Nuclei were stained with DAPI (blue). Scale bar, 20 μm. (G) Distributions of 2B11-positive neuron (•), glial cell (○), and dystrophic neurite cluster (▲) in the brain of 36-c. W, white matter; ST, superior temporal gyrus; MT, middle temporal gyrus; Am, amygdala; CS, collateral sulcus.

Table 2 – Glial immunoreactivities with 2B11 in the brains.

	17-a	19-a	26-a	26-b	32-a	32-c	36-c
Temporal cortex	–/+	+	+	++	+	+++	+
Hippocampus	–/+	–/+	+	NE	+	++	NE

The analysis for counting the number of 2B11-positive glial cells was performed as described in Experimental procedures. The number of 2B11-immunoreactive glial cells per mm^2 is indicated as follows: –/+, 1 to 30; +, 31 to 100; ++, 101 to 300; +++, 300 <; NE, not examined.

and hippocampi of animals over the age of 20. Whereas Gallyas silver staining was absent in the samples of 26-a, 26-b, and 32-a, argyrophilic tangles were detected in a neuron of the temporal cortex of 32-c (Fig. 4E). In the temporal cortex of 36-c, a moderate number of argyrophilic tangles was found in neurons, glial cells, and clustered dystrophic neurites by Gallyas silver staining (Figs. 4F, G). Almost all of them were located at the medial temporal areas adjacent to the amygdala (Fig. 4H). Distribution patterns of AT8 immunoreactivity and Gallyas silver staining in the brains of 32-a, 32-c, and 36-c are shown in Fig. 4H.

To examine the formation of paired helical filament (PHF), which is a unit fibril of NFT, in the monkey brains, we biochemically investigated the insoluble tau on the hippocampus of the animals aged 6, 17, 19, 25, and 32 years. However, we could not detect PHF even in the brain of the animal aged 32 years, 32-c (data not shown).

3. Discussion

Here, we showed that Aβ deposition occurred in cynomolgus monkey brains in age-dependent and region-specific manners, essentially resembling the deposition behavior of Aβ in human brains, both in normally aged individuals and patients with AD. The accumulation of phosphorylated tau was also observed; however, it started with poor correlation to the levels of Aβ deposition in the brain. Notably, Alzheimer-type tau pathology, including the formation of argyrophilic tangles and tau-accumulated dystrophic neurites, emerged predominantly in the medial temporal regions, and to a lesser extent, in the temporal cortices of the brains of advanced aged animals, which showed extremely high levels of Aβ deposition. The present findings make it attractive to use aged cynomolgus monkey brains to elucidate the mechanism and pathological significance of Aβ and tau pathologies.

In AD brains, it has been reported that the frontal and temporal cortices are the initial and favorable regions for Aβ deposition, whereas the occipital cortex and cerebellum are unfavorable regions for Aβ deposition (Braak and Braak, 1991; Näslund et al., 2000). The present study showed that the region specificity of age-dependent Aβ deposition in the monkey brains is similar to that of AD brain. In addition, extremely high levels of deposited Aβ were accompanied with rather low levels of soluble Aβ in the monkey brains as is the case in AD brains. It must be noted that the levels of soluble Aβ in the Tg mouse brains are extremely high compared with those in AD and monkey brains. Thus, although we do not intend to underestimate the usefulness of Tg mice to study Aβ pathogenesis, the use of nontransgenic animals, including cynomolgus monkey, is advantageous for studying the *bona fide* sequence of Aβ pathology, which can take place under particular conditions such as aging without the prior enhancement of Aβ production. In regard to the Aβ species that favorably deposits in the brains, attention has been paid to N3pE-Aβ (Hosoda et al., 1998; Iwatsubo et al., 1996; Saido et al., 1995, 1996). In the animals including transgenic mice, N3pE-Aβ was detected although its level was not necessarily high in the brains (Kawarabayashi et al., 2001; Kuo et al., 2001; Tekirian et al., 1998). In this study, a significant level of deposited N3pE-Aβ was only detected in the advanced aged monkey brain. Thus, although previous studies suggest that N3pE-Aβ may be a species that is prone to initially deposit in AD brain (Hosoda et al., 1998; Iwatsubo et al., 1996; Saido et al., 1995, 1996), our result suggests that, at least in monkey brains, N3pE-Aβ is generated by the conversion of the full-length Aβ following its deposition.

One of the interesting findings of this study is that the numbers of 2B11-positive neurons in the brains of animals over age of 30 were smaller than those in the brain of a 19-year-old animal. In contrast to this, the numbers of 2B11-positive oligodendroglial cells increased with age. Although we cannot exclude the possibility that the 19-year-old animal was an unusual case, it may be possible to speculate that the reduction of the 2B11 immunoreactivity in neurons reflects the failure of recognition by 2B11 owing to the conformational change of tau at its epitope region. In support of this possibility, it is noteworthy that tau likely adopts a specific conformation under the pathological condition (Jeganathan et al., 2008) or/and begins to assemble based on the particular sequence motif, ^{306}VQIVYK^{311}, which is included in the 2B11 epitope region (Von Bergen et al., 2000). If this is the case, we can explain why neurofibrillary tangle formation preferably occurs in neurons but not in glial cells in AD brains. In this

Fig. 4 – Accumulation of phosphorylated tau and formation of argyrophilic structure in the temporal cortices of advanced aged monkey brains. (A–D) Immunohistochemistry of the temporal cortices using AT8 with counterstaining using hematoxylin. (A) Faint AT8-positive glial cells (allows) of 26-b. (B) Strong AT8-positive glial cells and dystrophic neurites (inset) of 32-a. (C) Faint AT8-positive glial cells (arrows) and AT8-positive dystrophic neurite cluster (indicated by arrowheads) of 32-c. (D) Strong AT8-positive neurons of 36-c. (E–G) Gallyas silver staining. (E) A neuron with Gallyas-silver-positive structures of 32-c. (F) A neuron with Gallyas-silver-positive structures of 36-c. (G) A glial cell (arrow) and dystrophic neurite cluster (indicated by arrowheads) of 36-c. Scale bar, 20 μm. (H) Distributions of AT8-positive neuron (•), glial cell (○), dystrophic neurite (r), dystrophic neurite cluster (▲), Gallyas-silver-positive neuron (■), glial cell (·), and dystrophic neurite cluster (★) in the brains of 32-a, 32-c, and 36-c. W, white matter; ST, superior temporal gyrus; MT, middle temporal gyrus; Am, amygdala; Hi, hippocampus; CS, collateral sulcus.

context, a challenging and intriguing subject in future studies is to elucidate how the 2B11 epitope is involved in tau assembly and why the conformational change at the region of the 2B11 epitope selectively occurs in the intraneuronal milieu. A previous study showed that casein kinase 1, which is one of the expected tau protein kinases, is associated with NFTs but not with tau-containing glial inclusions in the brain with tauopathy including AD (Schwab et al., 2000). Given this

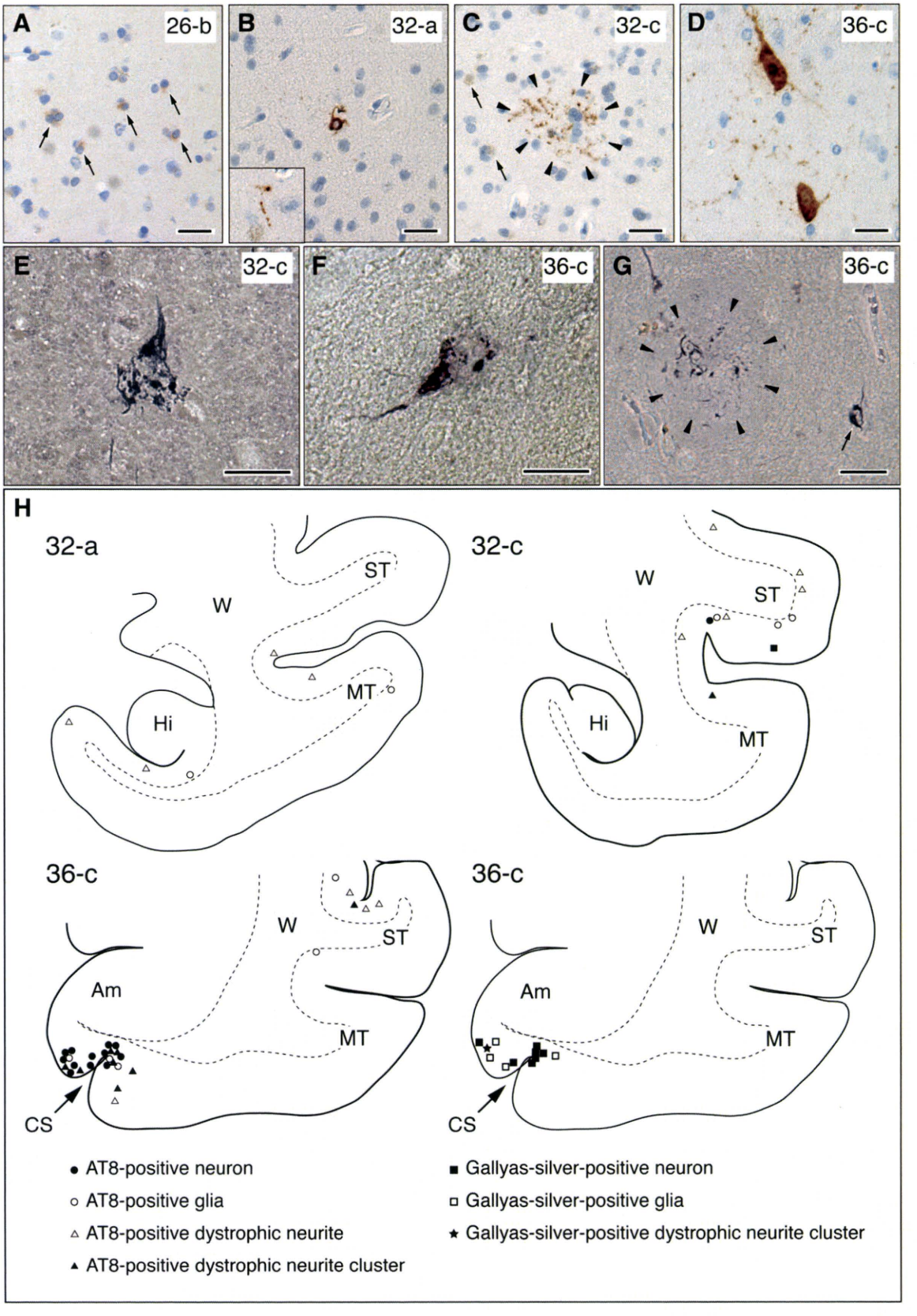

line of evidence, it is likely that the sequence of tau assembly, leading to the formation of pathological inclusions, is different between neurons and glial cells.

In the field of AD research, the amyloid cascade hypothesis has been widely accepted (Hardy and Higgins, 1992). In this hypothesis, it is argued that Aβ as amyloid induces the subsequent pathological events, including synaptic dysfunction, accumulation of phosphorylated tau as neurofibrillary tangles, and neuronal death. In this study, the accumulation of phosphorylated tau, which was determined by the mobility shift of the bands that reacted with 2B11, did not temporally correlate with the accumulation of insoluble Aβ, at least in the brains of animals younger than age 30. Thus, it is likely that the accumulation of phosphorylated tau merely reflects age-dependent perturbation of tau metabolism but not the amyloid-induced pathological sequence. However, Alzheimer-type tau pathology, including argyrophilic tangle formation and tau-accumulated dystrophic neurite formation, was observed in the neocortical areas of the advanced aged animals, which showed substantial amounts of insoluble Aβ in the same areas, although this tau pathology appeared to be of lesser extent than that in the medial temporal areas, in which Alzheimer-type tau pathology initially and favorably occurs (Braak and Braak, 1991). Thus, although further studies are required, it may be possible to assume that the emergence of intraneuronal tau pathology in the neocortices is a sequence downstream from the occurrence of extraneuronal Aβ deposition, which may be potentially responsible for various biological events, including massive inflammatory responses (Leung et al., 2009; Sheng et al., 1997) and release of toxic Aβ oligomers (Martins et al., 2008).

To date, substantial efforts have been paid to establish animal models to elucidate the pathogenesis of AD using transgenic and nontransgenic species, which likely complement each other. In nontransgenic models, it is interesting to note that age-dependent tau pathology such as the formation of argyrophilic inclusions was favorably observed in nonprimate species, such as sheep and bear. In contrast, primates are rather resistant to the development of tau pathology as long as the animals are allowed to age naturally without any insults to the brain (Table 3). To our knowledge, one of the exceptional primates, which develops significant tau pathology, is the baboon (Schultz et al., 2000a,b). Careful characterization of tau pathology in aged baboons was previously performed and provided evidence that abnormally phosphorylated tau accumulated in neurons, oligodendroglial cells, and

Table 3 – Summary of the studies on Alzheimer's disease-related proteins, Aβ and tau, in non human mammalian brains.

Animal	Aβ deposition	Tau accumulation	NFT formation [a]	References
Dog	+	+	ND	Braak et al., 1994; Cummings et al., 1993, 1996a,b; Czasch et al., 2006; Head et al., 2005; Papaioannou et al., 2001; Pugliese et al., 2006; Selkoe et al., 1987; Wegiel et al., 1998
Cat	+	+	ND	Braak et al., 1994; Cummings et al., 1996b; Head et al., 2005; Nakamura et al., 1996a,b
Rabbit	NE	+	NE	Härtig et al., 2000
Goat	ND	+	ND	Braak et al., 1994
Sheep	ND	+	+	Braak et al., 1994; Nelson et al., 1994
Bison	NE	+	+	Härtig et al., 2001
Guanaco	NE	+	NE	Härtig et al., 2000
Reindeer	NE	+	NE	Härtig et al., 2000
Bear	+	+	+	Cork et al., 1988; Härtig et al., 2000; Selkoe et al., 1987
Wolverine	+	+	NE	Roertgen et al., 1996
Lemurian	+	+	NE	Bons et al., 1991, 1995, 2006; Delacourte et al., 1995; Giannakopoulos et al., 1997; Härtig et al., 2000
Marmoset	+	+	ND	Geula et al., 2002; Palazzi et al., 2006; Ridley et al., 2006
Tamarin	+	ND	NE	Lemere et al., 2008
Squirrel monkey	+	ND	NE	Sawamura et al., 1997; Selkoe et al., 1987; Walker et al., 1987, 1990
Rhesus monkey	+	+	ND	Cork et al., 1990; Gearing et al., 1994, 1996; Geula et al., 1998; Härtig et al., 2000; Selkoe et al., 1987; Uno et al., 1996; Wisniewski et al., 1973
Cynomolgus monkey	+	+	+[b]	Kiatipattanasakul et al., 2000; Kimura et al., 2003, 2007; Nakamura et al., 1995, 1996a,b, 1998; Podlisny et al., 1991
Velvet	+	+	NE	Lemere et al., 2004
Baboon	+	+	+	Härtig et al., 2000; Schultz et al., 2000a,b
Chimpanzee	+	+[c]	+[c]	Gearing et al., 1994, 1996; Rosen et al., 2008
Orangutan	+	ND	ND	Gearing et al., 1997; Selkoe et al., 1987
Cynomolgus monkey	+	+	+	Present study

ND, not detected; NE, not examined.

[a] NFT (neurofibrillary tangle) formation confirmed by Gallyas silver staining or electron microscopy observation.

[b] Some neurons and glial cells were Gallyas-silver-positive in subcortical regions of the brain of one aged monkey, which appeared to suffer from a neurodegenerative disease such as progressive supranuclear palsy.

[c] Tau accumulation and tangle formation were observed in the stroke-affected area.

astrocytes, which were not affected in the cynomolgus monkey brains as shown in this study (Schultz et al., 2000a). Importantly, medial temporal areas are preferable for the development of tau pathology whereas neocortical areas are devoid of it even in the aged baboon (Schultz et al., 2000b). Although the difference in cell specificity for the development of tau pathology between the two species remains to be determined, the predilection of tau pathology to the medial temporal area was also the case for the cynomolgus monkey brains. Thus, the development of tau pathology in the neocortical areas is not likely due to aging-induced perturbation of tau metabolism, which may be background to the development of tau pathology in particular regions such as medial temporal areas, but may be attributed to the significant Aβ deposition in these areas.

In conclusion, the present study demonstrates the value of aged cynomolgus monkey brains to elucidate the *bona fide* sequence of Alzheimer-type pathology, including extraneuronal Aβ deposition and intraneuronal tau accumulation, and furthermore to explore whether these two pathological events are related or independent of each other.

4. Experimental procedures

4.1. Animals

Thirty-four cynomolgus monkey (*Macaca fascicularis*) brains, the ages at death were from 6 to 36 years, were examined in this study (Supplemental Table 1). Postmortem delay ranged from 1 to 2 h. The frontal, temporal, and occipital cortices, hippocampus, and cerebellum of the brains were used for biochemical analysis, and the temporal cortex and hippocampus were used for immunohistochemical analysis. All the brains were obtained from the Tsukuba Primate Research Center, National Institute of Biomedical Innovation, Japan. All the animals were housed in individual cages and maintained in accordance with the National Institute of Biomedical Innovation rules and guidelines for experimental animal welfare. Three monkeys (age: 26 ($N=1$) and 36 ($N=2$) years) died of natural causes. The remaining animals were deeply anesthetized with a lethal dose of pentobarbital prior to brain extraction. Supplemental Table 1 summarizes the profiles of the examined animals and indicates which subject was used for what analysis. Tissue blocks were fixed (see below) and embedded in paraffin for sectioning (for immunohistochemical studies) or snap frozen and stored at −80 °C until use (for biochemical studies). Based on the fact that SP formation is naturally and consistently observed from age around 25 years (Nakamura et al., 1998) also regarding the life expectancy of this animal species, the animals over the age of mid-20s can be mentioned as aged ones. In addition to monkey samples, brain tissue of two APP-Tg (Tg2576) mice (age: 13.5 months) was subjected to the biochemical analysis of Aβ.

4.2. Antibodies

We used the following antibodies: a mouse monoclonal anti-Aβ antibody, 6E10 (epitope within residues 3–8) (Covance, Dedham, MA); a rabbit polyclonal anti-Aβ antibody, anti-human amyloid β (N) (raised against synthetic peptide of the amino-terminal part of Aβ) (IBL, Gunma, Japan); a mouse monoclonal anti-Aβ40 antibody, 1A10 (raised against synthetic peptide of the residues Aβ35–40) (IBL); a rabbit polyclonal anti-Aβ42 antibody (raised against synthetic peptide of the carboxy-terminal part of Aβ42) (IBL); a rabbit polyclonal anti-Aβ (N3pE-42) antibody (raised against synthetic peptide of the amino-terminal part of Aβ in which the third amino-terminal glutamate is converted to pyroglutamate) (IBL); three mouse monoclonal anti-tau antibodies, 2B11 (epitope, residues 301–312) (IBL), HT7 (epitope, residues 159–163) (Thermo Scientific, Rockford, IL); a monoclonal anti-phosphorylated tau antibody, AT8 (epitope, phosphoSer-202 and phosphoThr-205) (Innogenetics NV, Gent, Belgium); a rabbit polyclonal anti-GFAP antibody (Zymed, South San Francisco, CA); and a rabbit polyclonal anti-Olig2 antibody (IBL), which react with the nuclear protein, Olig2, of oligodendrocytes.

4.3. Sample preparation

Each of the frozen tissues was homogenized using a Dounce homogenizer with 30 strokes on ice in 19 volumes of Tris-buffered saline (TBS: 50 mM Tris–HCl, pH 7.4, 150 mM NaCl) containing Complete™ protease inhibitor cocktail (Roche Diagnostics, Mannheim, Germany). The TBS-soluble fraction was collected by ultracentrifugation of the homogenate at 436,000×*g* for 15 min at 4 °C. For the detection of TBS-insoluble Aβ, the pellet was washed twice with TBS by sonication, delipidated with chloroform/methanol (1:2; v/v) by brief sonication and then incubated for 15 min at room temperature (RT). After the centrifugation at 20,400×*g* for 20 min, the pellet was solubilized in 100% formic acid, followed by incubation for 1 h at RT. The supernatant, which was collected by the centrifugation of the homogenate at 20,400×*g* for 20 min, was dried using speed vac (TOMY SEIKO, Tokyo, Japan). The resultant pellet was used for the study of TBS-insoluble Aβ. In the study of tau, the TBS-soluble fraction was prepared in the same manner as that for Aβ except for the use of phosphatase inhibitors, including 20 mM NaF, 25 mM $Na_4P_2O_7$, 1 mM β-glycerophosphate, 1 mM Na_3VO_4, and 1 μM okadaic acid, in homogenization buffer. In the Western blotting for TBS-soluble tau, the heat-stable fraction was collected by boiling the samples for 10 min at 95 °C in 2% β-mercaptoethanol, 480 mM NaCl, followed by centrifugation at 20,400×*g* for 20 min at 4 °C. The resultant supernatants were subjected to Western blotting. The dephosphorylation of TBS-soluble tau was performed as previously described (Miyasaka et al., 2001). The samples were incubated in 50% ammonium sulfate for 30 min on ice. After the centrifugation of the samples at 20,400×*g* for 15 min at 4 °C, the precipitated proteins were suspended in a buffer containing 50 mM Tris–HCl, pH 8.7, protease inhibitor cocktail, and 10 U/ml *E. coli* alkaline phosphatase (Type III, Sigma, St. Louis, MO). The samples were incubated at 67 °C for 3 h. For the analysis of TBS-insoluble tau, TBS-insoluble materials were processed as described elsewhere (Lee et al., 1999) with some modifications. TBS-insoluble precipitate was homogenized in 20 volumes of Tris buffer (50 mM Tris–HCl, pH 7.4, 0.8 M NaCl, 10% sucrose) containing Complete™ protease inhibitor cocktail and the phosphatase inhibitors with a motor-driven Teflon homo-